MULTIWAVELENGTH LASER PROPAGATION STUDY -- III

Quarterly Progress Report No. 2
September 16, 1970 - December 15, 1970

J. Richard Kerr

Oregon Graduate Center
for Study and Research
Portland, Oregon

January, 1971

Sponsored by

Advanced Research Projects Agency
ARPA Order No. 306

DISCLAIMER NOTICE

THIS DOCUMENT IS THE BEST QUALITY AVAILABLE.

COPY FURNISHED CONTAINED A SIGNIFICANT NUMBER OF PAGES WHICH DO NOT REPRODUCE LEGIBLY.

ACKNOWLEDGEMENT

This research was supported by the Advanced Research Projects Agency of the Department of Defense, and was monitored by the Office of Naval Research under Contract N00014-68-0461-0001.

SUMMARY

An extensive experimental investigation of multiwavelength laser beam scintillations and atmospheric turbulence characteristics has been completed. It has been found that turbulence spectra approximate the inertial-subrange model only under conditions of strong turbulence, which corresponds with saturation of scintillations at visible and near-IR wavelengths. Hence, it is only at longer wavelengths (such as 10.6 microns) that Rytov analyses utilizing the inertial subrange have substantial value.

The saturation phenomenon occurs at the same scintillation levels independent of wavelength, and significant falloff of scintillation "beyond saturation" is observed. Covariance measurements show transverse amplitude correlation lengths which are significantly affected by strong turbulence; the correlation lengths increase at shorter wavelengths while decreasing at longer wavelengths, as turbulence increases. Receiver aperture-averaging results at visible wavelengths show that the large-aperture smoothing of total-signal fluctuations is much less effective than theoretically predicted, and confirm the especially-poor averaging in strong turbulence conditions.

CONTENTS

I. INTRODUCTION

During the present period, we have completed a substantial number of data-gathering "standard runs" under a wide variety of turbulence conditions. As defined previously, a standard run consists of the following:

1. Direct determination of the turbulence spectrum

2. Determination of the refractive index structure constant C_n^2

3. Measurement of the log amplitude scintillations over a short (500') path at 6328Å, including probability distribution

4. Measurement of the log amplitude scintillations over a nearly-one-mile path, simultaneously at 4880Å, 1.15μ, and 10.6μ, including probability distributions

5. Simultaneous three-wavelength measurement of the covariance

6. Simultaneous three-wavelength determination of the scintillation spectra

7. Measurement of receiver aperture-averaging of scintillations at 4880Å

8. Recording of general meteorological parameters.

In all cases, the optical transmitters (lasers) were arranged to provide virtual spherical-wave sources, to eliminate possible ambiguity in interpretation due to finite transmitter apertures. The receiver aperture of 3mm also represented a virtual point.

The principal conclusions may be summarized as follows:

1. The turbulence spectrum frequently fails to fit the Kolmogorov or inertial-subrange prediction, even approximately.

2. Theoretical predictions of scintillations based on the usual combination of the Kolmogorov model and Rytov perturbation analysis are severely limited in their utility, especially at shorter (visible and near-IR) wavelengths.

3. Although a longer path will be required for final confirmation at 10.6μ, it strongly appears that saturation of scintillations occurs at the same level of log amplitude variance regardless of wavelength,

4. The covariance and receiver aperture-averaging vary significantly with turbulence characteristics.

5. Receiver aperture averaging is usually much less effective than predicted by theory.

These statements, of course, involve oversimplifications, and will be expanded upon in a later section.

In Section II, the experimental methodology will be briefly reviewed. In Section III, the results will be summarized and the implications discussed. Future plans will be reviewed in Section IV.

II. EXPERIMENTAL APPROACH AND EXAMPLES

In this section, certain pertinent factors in the experimental methodology will be reviewed and examples of particular results will be given. However, the reader is referred to previous reports[1] for detailed descriptions of the experimental setup and instrumentation.

A. Structure Constant C_n^2

The refractive index structure constant[2] was measured using a low-noise, feedback-stabilized, subcarrier bridge system with fast thermal microprobes and a five-minute averaging time. The probe separation was 10 cm and the height was approximately that of the optical beam (two meters). The values of C_n^2 which are actually deduced are, of course, of limited meaning when the turbulence spectrum fails to fit the Kolmogorov model;[2] however, for a given average temperature and barometric pressure, C_n^2 is essentially proportional to $\langle(\Delta T_{12})^2\rangle$ and therefore represents some indication of the strength of turbulence. Because of this and also the customary use of the quantity in other investigations, we retain C_n^2 when summarizing the results in Sec. III.

In earlier reports, we have described the quasi-log-normal nature of ΔT, and pointed out that this "intermittency" has been discussed in the literature.[3,4] It now appears that our earlier question as to the effect of this intermittency on the validity of the theory (specifically, the assumption of local homogeneity[5]) was largely unnecessary: there is no clear indication that C_n^2 predicts too large a scintillation level except in the saturated region.[2] However, the question of abrupt interfaces between low and high turbulence regions merits further investigation.[6]

It may be pointed out that C_n^2 is a weak function of wavelength. Hence, whenever values of C_n^2 are given in later sections, it will be understood that the reference wavelength is 4880Å.

B. Turbulence Spectrum

The spatial spectrum of the turbulence was determined with a single thermal microprobe in the system described above, utilized in conjunction with an excellent low-frequency spectrum analyzer. Specifically, the analog voltage representing $(T(t) - \langle T \rangle)$ was recorded for five minutes on an FM instrumentation recorder, and this five minute "time window" was later utilized for spectral analysis at logarithmically-spaced, discrete frequencies with full five-minute averaging on each. In this manner, the effects of nonstationarity in the turbulence are eliminated. A log-log plot of this spectrum then yields the one-dimensional turbulence spectrum.[7]

In literally all cases, it was found that the spectra followed one or two power laws (straight lines on log-log plots) with definite breakpoints. A breakpoint may be interpreted as a manifestation of an "inner scale", and the size of this scale may then be computed from the average wind velocity. This computation is highly approximate under variable wind conditions.

An example of a turbulence spectrum which approximates the Kolmogorov model is shown in Fig. 1a. The inertial subrange prediction is for a slope of $-5/6 = -0.833$ for the rms spectrum, and the example shown gives a slope of -0.79 with no breakpoint. Figure 1b shows an example of a higher slope (-0.958) with a breakpoint, and Fig. 1c shows a lower slope (-0.55). Finally, Fig. 1d shows a slope of (-0.75) with a breakpoint.

C. Log Amplitude Scintillation Measurements

Using very-large-dynamic-range electronics as described previously, the log amplitude variance was simultaneously measured at all wavelengths in a special-purpose analog computer with five-minute averaging. More importantly, the probability distributions of log-amplitude were directly and simultaneously obtained. The inverse Fresnel number of the transmitter is $\sim 10^4$ at 4880Å and $\sim 10^2$ at 10.6μ. At 1.15μ, the highly multimode beam also approximates a point source.

During conditions of quasi-stationarity of the turbulence and hence scintillation statistics, the log amplitude probability distribution is gaussian, at least to the resolution of the present method. The slope then yields the log amplitude variance (Fig. 2a), which typically agrees to within a few percent of the computer-output value. However, since the probability determination takes several minutes, a non-log-normal plot can result (Fig. 2b) during non-stationarity conditions. In this case, a suitable average slope is taken, and the computer output is checked for verification.

We intend later to investigate the exact log-normality of the scintillations in more detail. Stationarity effects will be eliminated through the technique referred to in Section II.B above; we will record the log amplitude scintillations for several minutes and then analyze discrete probability points, each averaged over this common "time window."

One effect which was noted at very low scintillation levels was that of beam wander due to atmospheric refraction. That is, with low scintillations, a "virtual scintillation" results from the changing average power at the receiver. Usually, this may be ignored through an appropriate choice of the low-frequency cut-off of the signal representing log $(A/\bar{A})$,

e.g. 1 Hz. However, it was occasionally true at low wind velocities and the IR wavelengths that the true scintillation spectra somewhat overlapped this effect.

For later reference, the theoretical prediction of log amplitude variance is[2]

$$\sigma^2 = 0.124\, C_n^2\, k^{7/6}\, L^{11/6}, \qquad (1)$$

where k is the optical-IR wavenumber and L is the pathlength.

D. Log Amplitude Covariance Measurements

Cross-correlation of the log amplitude taken at two horizontally-spaced receivers was utilized to determine the covariance. This was again performed simultaneously at the three wavelengths, with sequential, discrete separations and one-minute averaging times (Fig. 3). Nonstationary conditions occasionally resulted in some distortion of the resultant curves (Fig. 4). In all cases, the characteristic transverse log amplitude correlation length r_a was defined as the 1/e point of the covariance curve (normalized to the variance).

Since the computer and recorder output level corresponding to zero correlation is subject to small zero-drifts, this level was determined with uncorrelated test signals prior to each run.

E. Scintillation Spectrum Measurements

The amplitude scintillations at the three wavelengths were simultaneously recorded on the instrumentation recorder, and then later analyzed utilizing a three-minute sweep time on the low-frequency spectrum

instrument (Fig. 5). It is recognized that a much more meaningful plot involves fW (f), where W is the spectral density and f is the frequency, and such measurements are planned later in this program. For the present purposes, an approximate 1/e point was determined relative to the low-frequency peak, and this "spectral width" was compared with r_a (Sec. II.D above) to test the hypothesis of "frozen-in turbulence".[2]

F. Aperture Averaging Measurements

Utilizing a 12.5-inch parabolic mirror, the log amplitude variance vs. receiver aperture was determined at 4880Å. The computer was employed directly, and discrete apertures from near-zero to full (with a small center obstacle) were employed with one-minute averaging for each. A high degree of averaging is illustrated in Fig. 6a, where the corresponding covariance curve is also shown; a relatively-low degree of averaging is shown in Fig. 6b. In all cases, the total optical power on the detector was maintained well within its linear region, and image dancing effects were eliminated through the use of defocusing onto a large-cathode photomultiplier. The results agreed with those obtained from a small silicon photodiode.

G. Time Record of Scintillations

As a side point, we show in Figure 7 a simultaneous time record of log amplitude variance at the three wavelengths, and the corresponding value of thermally-determined C_n^2, all with ten-second averaging times. In a recent report,[8] we showed an example of well-correlated but varying scintillations as large, broken clouds alternately exposed and shaded the path. In the present example, the nonstationarity was due to less obvious reasons, and the correlations between respective wavelengths and C_n^2 are poor.

The theory predicts that log amplitude variances will be identically affected by nonuniformities, regardless of wavelength.[2]

$$\sigma^2 = 0.14\, k^{7/6} \int_0^L C_n^2(Z) \left(\frac{Z}{L}\right)^{5/6} (L-Z)^{5/6}\, dZ \qquad (2)$$

That is, k is outside the integral. Hence, we must conclude that the effect illustrated in Figure 7 is a manifestation of a continually changing and non-uniform turbulence spectrum over the path, such that the interaction of the optical filter function[9] at each wavelength with this spectrum produces essentially uncorrelated results. Since the turbulence spectral slope was measured as (-0.55) at one time during this run, the spectrum was indeed highly non-inertial.

III. SUMMARY OF RESULTS AND CONCLUSIONS

A. Turbulence Spectrum

In Fig. 8, we show the values of turbulence spectral slopes (e.g. Fig. 1) and inner scales for the standard runs, as a function of "C_n^2" (see Sec. II.A). The slopes tend more nearly to the inertial subrange value (line shown in Fig. 8) as the strength of turbulence increases, and at weaker turbulence levels tend to be mostly smaller than this value. This has been interpreted[2] as representing an energy input within this scale range. There are, however, a number of examples with significantly larger slopes, possibly indicating dissipation. The overall range encompassed by the slopes is approximately -0.5 to -1.4, and even at these extremes, a define power-law behavior is evident.

There is apparently some tendency for the inner scales to become smaller as turbulence increases and slopes more nearly approximate the inertial value. In some cases, these scales are so large that their meaning becomes nebulous, except as breakpoints between two power-law regions of the spectra.

In Fig. 9, the wind velocity is shown vs. C_n^2, and no particular relationship is evident.

In Fig. 10, the slopes and inner scales are shown vs. wind velocity; it is seen that the inner scales tend to zero as velocities increase, and large slopes are confined to low velocities.

In Fig. 11, we show the slopes and inner scales vs. time of day for each run. This plot is of somewhat limited meaning due to the six-month time-span of the measurements, but does show that erratic turbulence spectra tend to occur during sunrise and sunset periods.[10] (Simple night-time measurements have shown low turbulence and similar erratic behavior). It may also be noticed that clear-weather spectra tended to be more nearly inertial; this corresponds with higher turbulence conditions, as shown in Fig. 12.

Finally, in Fig. 13, we show the slope of the spectrum inside the inner scale, vs. wind velocity. Good power-law behavior was evidenced in this region, which is contrary to Tatarski's assumption of an exponential behavior.[5] These slopes are highly variable from time to time, and are quite important in those cases where the "inner scale" or breakpoint occurs at sufficiently large scales that the optical filter function (at least at the visible and near-IR wavelengths) will strongly interact within this region.

In Fig. 13, and further figures, we arbitrarily define a "good inertial spectrum" as follows:

> Slope (outside the inner scale) between -0.72 and -0.94
> Inner scale or breakpoint corresponding to less than one-half the theoretical value of r_a at each wavelength

It is then apparent from Fig. 13 that, inside the breakpoint, larger slopes (more rapid energy fall-off with increasing wavenumber) correspond to more nearly inertial conditions.

The conclusions that may be drawn from the data of this section are that

(1) Much more work in atmospheric physics per se is needed to attempt to correlate turbulence spectral behavior with overall conditions

(2) Non-inertial behavior is very common except at high turbulence levels; hence, the usual theoretical approaches are of limited utility

(3) Given a turbulence spectral characteristic, the optical filter function analysis can in principle yield theoretical scintillation predictions;[9] the important characteristics may include the region inside the inner scale.

B. Results of Short-Path Scintillation Measurements

In an attempt to obtain an optical indication of C_n^2 which is free of possible effects from saturation,[11] we included in each standard

run a measurement of log amplitude variance at 6328Å for a point source at 500'. In over 90% of the runs, this measurement yielded scintillations substantially below those predicted from the thermal C_n^2 measurement and Eq. (1). However, due to the shortness of this path, the appropriate relationship is[2]

$$\sigma^2 = 0.32\, C_n^2\, L^3\, l_o^{-7/3} \qquad (L \ll l_o^2/\lambda) \qquad (3)$$

where l_o is the inner scale.

We have utilized this relationship to infer an inner scale:

$$l_o^{7/3} = 1.13 \times 10^6 \, \frac{C_n^2}{\sigma^2} \quad (\text{meters})^{7/3}, \qquad (4)$$

where C_n^2 is as obtained thermally, and σ^2 is the measured 6328Å variance. These inner scales are shown along with the direct or thermally-determined scales, vs. wind velocity in Fig. 14. It should be pointed out that, at higher wind velocities and using the thermal technique, small inner scales may be taken as zero due to the high frequency of the corresponding breakpoint. The approximate lower limit on a discernible inner scale is

$$\text{Minimum discernible scale (cm)} \approx \frac{\text{wind speed (mph)}}{10}$$

For real scales smaller than this, the scale will be inferred to be zero.

Even though the theoretical basis for deriving Eq. (3) is poorly satisfied in the real atmosphere, we may note a scaled correlation between the inner scales determined by the two methods. This is evident in Fig. 15, where the left or 0.1 cm abscissa is taken as virtual zero.

C. Multiwavelength Log Amplitude Variances

The experimental values for log amplitude variance are plotted in Figs. 16a,b,c, vs. theoretical predictions, where the theoretical values are obtained from the thermal C_n^2 and Eq. (1). The phenomenon of saturation and fall-off beyond saturation ("supersaturation") is evident at the two shorter wavelengths. In Figure 17, all three wavelengths are combined. At 10.6μ, saturation is apparently approached but never reached for this pathlength.

In the plots of Figs. 16 and 17, the points corresponding to a "good inertial spectrum" as defined above are distinguished from other data points. It is evident that the theoretical predictions are of very limited value at shorter wavelengths and reasonable pathlengths because saturation occurs when the turbulence is strong enough to have an inertial subrange. Hence, the theoretical deficiencies in the atmospheric model and in the propagation analyses respectively occur in opposite situations, and the theory is largely useless except at 10.6μ. This is a very important point.

Since the path used in these experiments is nearly but not totally uniform, with a beam height above ground that varies irregularly by approximately 2/3 of a meter over the path, the effective average value of C_n^2 (Eq. 2) is somewhat in doubt. Hence, the theoretical line in Figs. 16 and 17 may be shifted down slightly, representing a smaller average C_n^2 than that determined at the point of thermal measurement. The effect is equal at all wavelengths.

The experimental variances at 4880Å vs. 1.15μ and 4880Å vs. 10.6μ are shown in Fig. 18, along with the theoretical line from Eq.(1). Saturation and supersaturation are again evident, and involve most of the "good inertial spectrum" data points. It is evident that 1.15μ and 10.6μ

scintillations tend to be larger than theoretically predicted from the 4880Å values, even away from saturation of the lat er. This may relate to the noninertial turbulence spectra. The two points at lowest scintillation levels in the infrared probably represent beam wander.

The spread in points in Figs. 16-18 is due to the following reasons:

(1) The nonstationarity of atmospheric turbulence. Although broken-cloud days were eliminated in these data, the phenomena are fundamentally non-stationary

(2) The nonuniformity of the turbulence, including the turbulence spectrum

(3) The variation of the turbulence from the inertial model

(4) Beam wander effects comparable to scintillations at low turbulence levels (possibly involved in two or three points of lowest abscissa at 1.15μ and 10.6μ)

Factor number 1 requires further comment. Excluding the obvious case of broken clouds with variable heating from sunlight, the degree of turbulence tends to be highly variable on days of low wind velocity or (to a lesser extent) highly-variable wind velocity. At near-zero wind velocity, stationarity is to all practical purposes absent, since the frequencies of scintillations are so low (and hence required averaging times so long) that monotonic trends become very important. For more reasonable wind conditions, much longer averaging times may be used to reduce spread, but the

results then disguise short-term scintillation extremes which will be encountered by real operating systems.

D. Covariances

The three-wavelength covariance lengths r_a are shown vs. C_n^2 in Fig. 19. The abscissa is also shown in terms of corresponding theoretical variance at each respective wavelength. The theoretically predicted values of r_a [12] are also shown.

It is evident that in the region beyond saturation, the values of r_a increase substantially at the two shorter wavelengths; this is confirmed by poorer aperture averaging discussed below. However, at 10.6μ, the transverse correlation lengths decrease substantially at these turbulence levels. The latter result is surprising, since the (inertial subrange, non-saturated) theory is relatively good for these points.

As expected, the highly-anomalous points, e.g. at 10.6μ, correspond to highly anomalous turbulence spectra.

E. Scintillation Spectra and Frozen-In Turbulence

Although our method of determining a spectral "width" was approximate, it is interesting to plot the following quantity for each run:

$$\frac{r_{a_{\lambda_1}} \times \text{spectral width}_{\lambda_1}}{r_{a_{\lambda_2}} \times \text{spectral width}_{\lambda_2}}$$

According to the frozen-in hypothesis, this quantity should be unity.

The above ratio is plotted vs. wind velocity in Figs. 20a,b,c. Although the spread is fairly substantial due to the method, the hypothesis is generally confirmed.

F. Receiver Aperture Averaging

Aperture averaging may be characterized by the following quantity:

$$\frac{\text{log amplitude variance at full (12.5") aperture}}{\text{log amplitude variance at virtual point aperture}}$$

This quantity was determined at 4880Å and is plotted vs. theoretical (point-aperture) variance in Figure 21. It is seen that, as turbulence increases, aperture averaging becomes worse and becomes surprisingly ineffective in the strongly saturated region. Indeed, at all levels of turbulence, the reduction in scintillation is much poorer than simple theory would predict.[2] However, there are evident deficiencies in the theoretical treatments of this effect.[6,13] It may be noted that the effects of beam wander may be evident at the lowest turbulence levels.

Aperture averaging is plotted vs. r_a (4880Å) in Fig. 22. Although the degree of correlation in scintillations over the entire aperture is not given by simple knowledge of r_a, a relationship between r_a and degree of averaging is evident as expected.

It is clear that the performance of large-aperture receiver systems will be poorly predicted by existing aperture-averaging theory, and that a residual variance of 15-20% of the point-receiver value must be accommodated in system design.

IV. FUTURE PLANS

For the remainder of this program, the following experiments are planned:

(1) Investigation of transmitter aperture effects

(2) Further investigation of receiver aperture averaging

(3) Detailed investigation of scintillation probability distribution

(4) Investigation of scintillation spectra

In addition, we propose a follow-on phase in which the standard runs and other experiments will be conducted over a longer (e.g. 3 mile) path.

References

1. The reports on this program are as follows:
   Multiwavelength Laser Propagation Study-I
   Quarterly Reports 1,2,3
   Interim Final Report
   Multiwavelength Laser Propagation Study-II
   As above
   Multiwavelength Laser Propagation Study--III
   Quarterly Report No. 1

2. Robert S. Lawrence and John W. Strohbehn, "A Survey of Clear-Air Propagation Effects Relevant to Optical Communications," Proc. IEEE, vol. 58, October 1970, pp. 1523-1545.

3. Paul J. Titterton, Sylvania Electronics Systems (Western Operations), private communication.

4. A. S. Gurvich and A. M. Yaglom, "Breakdown of Eddies and Probability Distributions for Small-Scale Turbulence," Physics of Fluids Supplement (Boundary Layers and Turbulence), pp. 559-565, 1967.

   A. S. Gurvich, "Probability Distribution of the Square of the Temperature Difference between Two Points of a Turbulent Flow," Soviet Physics - Doklady, vol. 12(1), (Fluid Mechanics, pp. 17-20, July 1967).

   C. H. Gibson, G. R. Stegen, and R. B. Williams, "Statistics of the Fine Structure of Turbulent Velocity and Temperature Fields Measured at High Reynolds Number," J. Fluid Mechanics, vol. 41 part 1, pp. 153-167, 1970.

   R. W. Stewart, J. R. Wilson, and R. W. Burling, "Some Statistical Properties of Small Scale Turbulence in an Atmospheric Boundary Layer," J. Fluid Mechanics, vol. 41 part 1, pp. 141-152, 1970.

5. V. I. Tatarski, Wave Propagation in a Turbulent Medium, New York: 1961, McGraw-Hill.

6. Informal discussion during 1970 OSA Meeting, Hollywood, Florida. Meeting included E. Alcaraz, S. Clifford, S. Collins, R. Lawrence, P. Livingston, and G. Ochs.

7. Peter M. Livingston, NRL, private communication.

8. See reference 1, phase II, QPR 3, figure 11.

9. A. Ishimaru, "Fluctuations of a Beam Wave Propagating through a Locally Homogeneous Medium," Radio Science, vol. 4, pp. 295-305, April 1969.

Ishimaru, A, "Fluctuations of a Focused Beam Wave for Atmospheric Turbulence Probing," Proc. IEEE, vol. 57, April 1969, pp. 407-414.

F. P. Carlson, "Application of Optical Scintillation Measurements to Turbulence Diagnostics," JOSA, vol. 59, pp. 1343-1347, October 1969.

10. P. H. Deitz and N. J. Wright, "Saturation of Scintillation Magnitude in Near-Earth Optical Propagation," JOSA, vol. 59, pp. 527-535, May 1969.

11. D. L. Fried, et al, "Optical Propagation Measurements at Emerson Lake--1968," Final Report, Autonetics.

12. D. L. Fried, "Propagation of a Spherical Wave in a Turbulent Medium," JOSA, vol. 57, pp. 175-180, February 1967.

13. S. F. Clifford, ESSA, private communication.

List of Figures

17. Experimental vs. Theoretical Log Amplitude Variances--All Wavelengths

18. Experimental Log Amplitude Variances for Pairs of Wavelengths

19. Transverse Log Amplitude Correlation (Covariance) Lengths r_a vs. C_n^2

20. Ratios of r_a Xspectral width for pairs of wavelengths (see text, p. 14) vs. wind speed
    a. 1.15 microns/4880A
    b. 10.6 microns/4880A
    c. 10.6 microns/1.15 microns

21. Receiver Aperture-Averaging Percentage vs. Theoretical Log Amplitude Variance (4880A)

22. Receiver Aperture-Averaging Percentage vs. r_a (4880A)

Figure 10

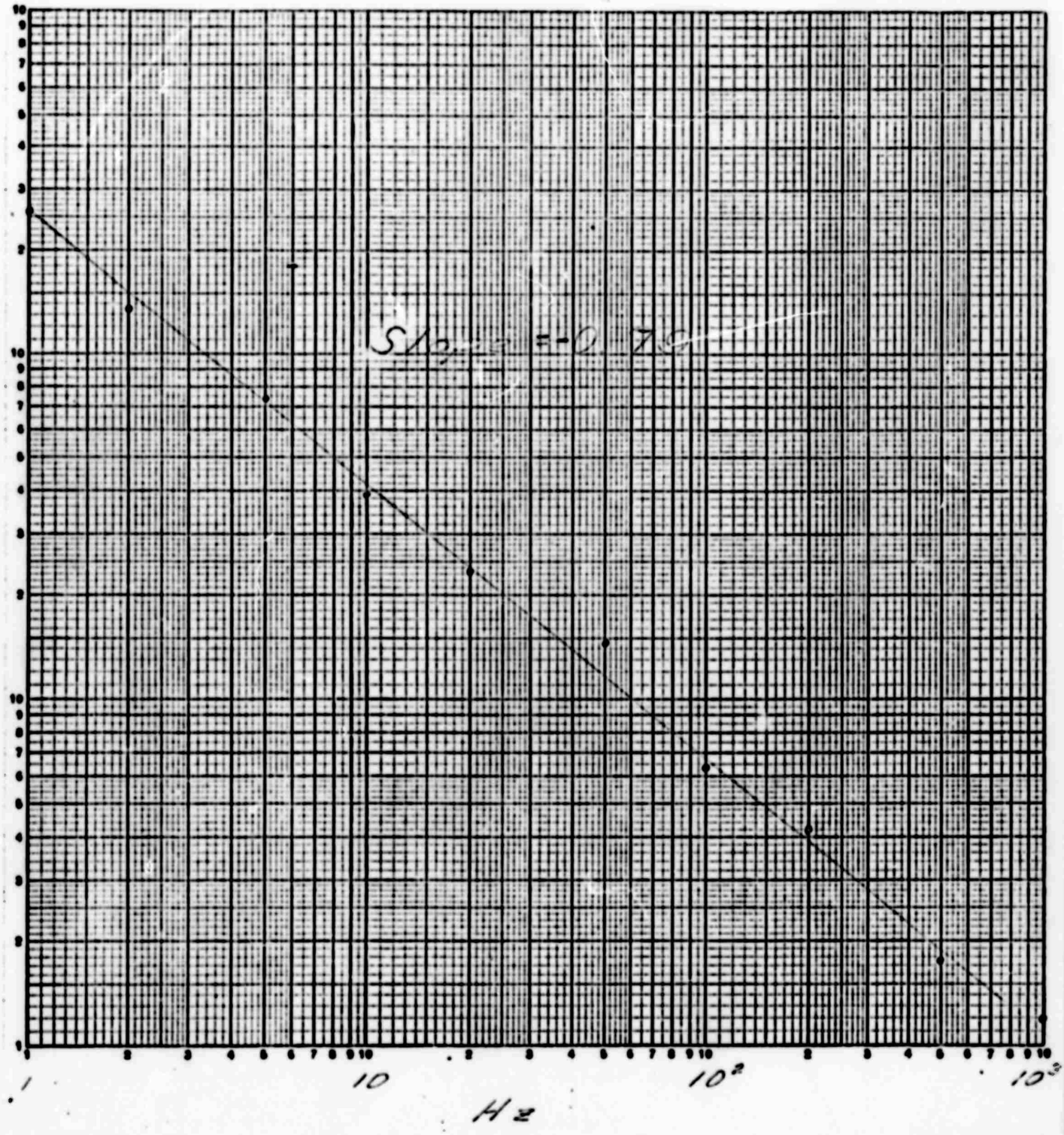

Figure 16

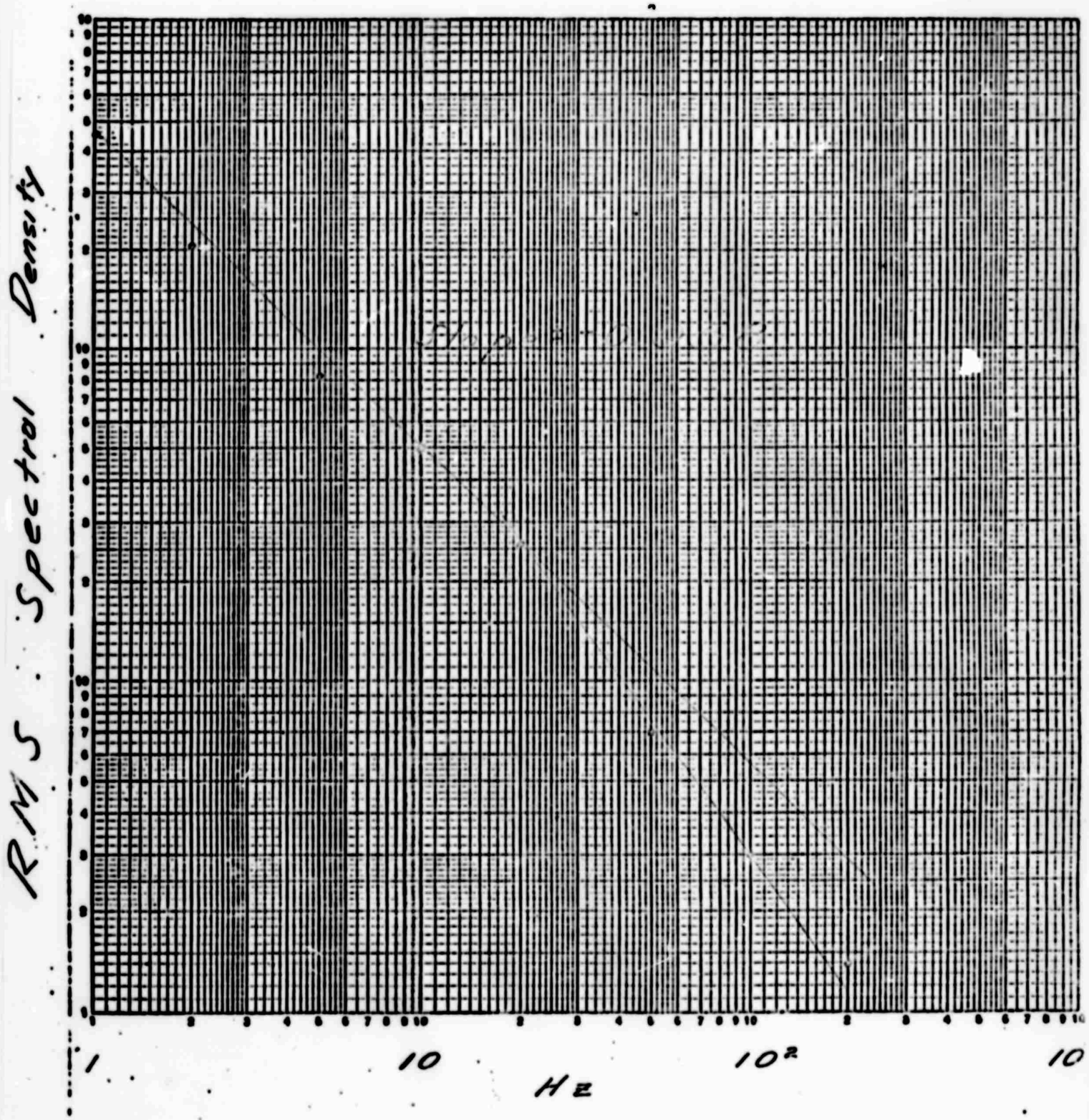

Figure 1c

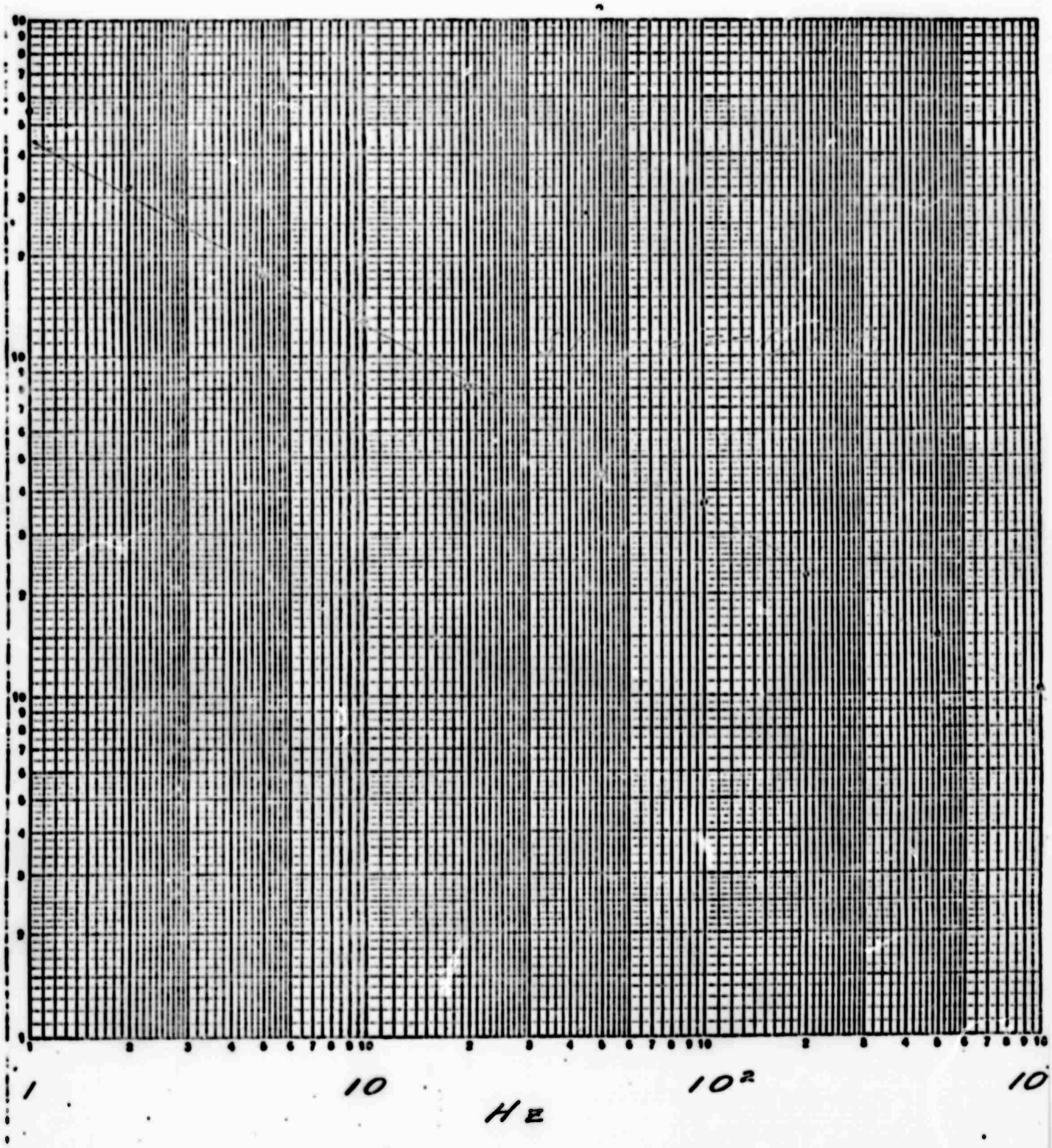

Figure 1d

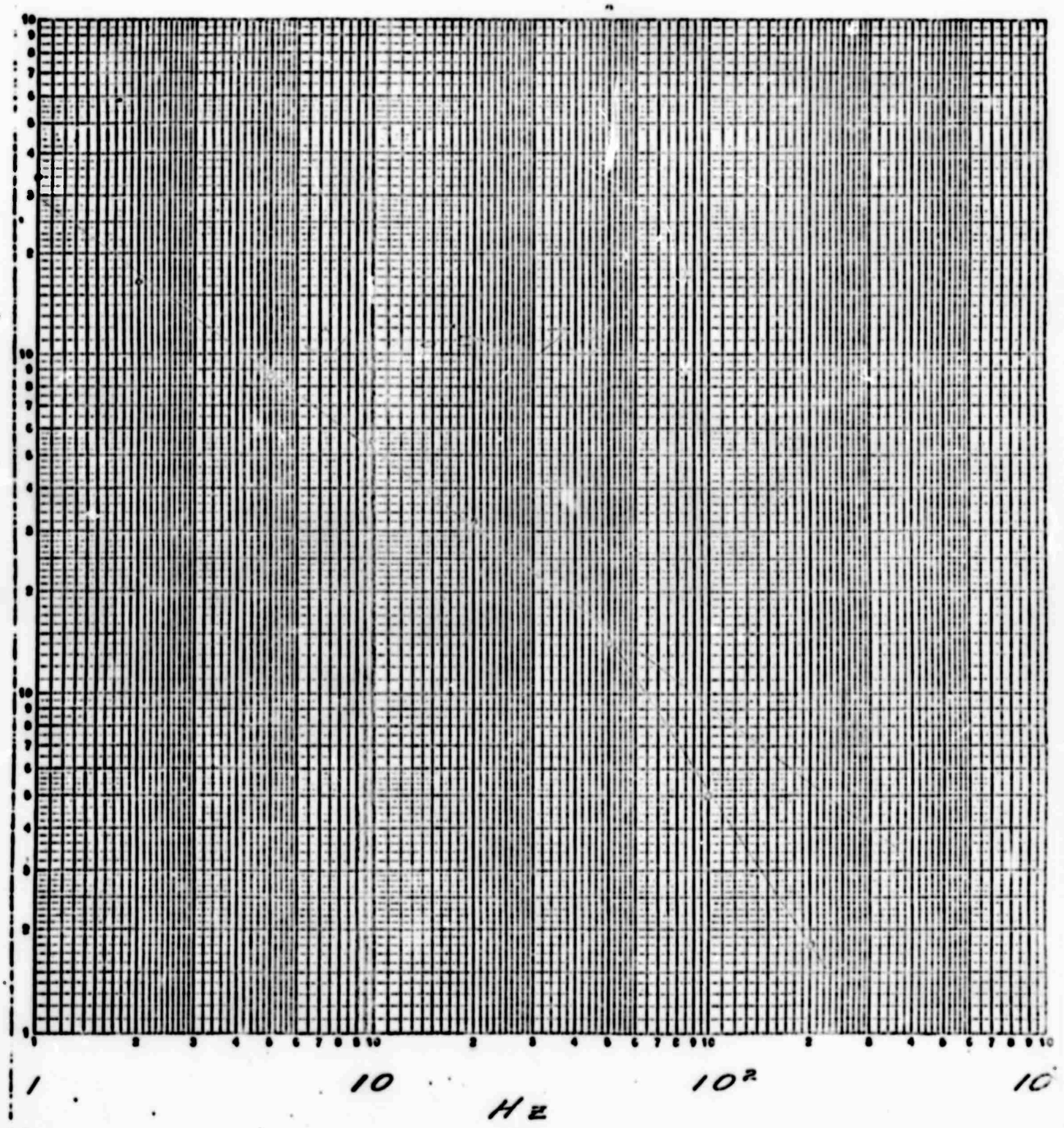

Figure 2a

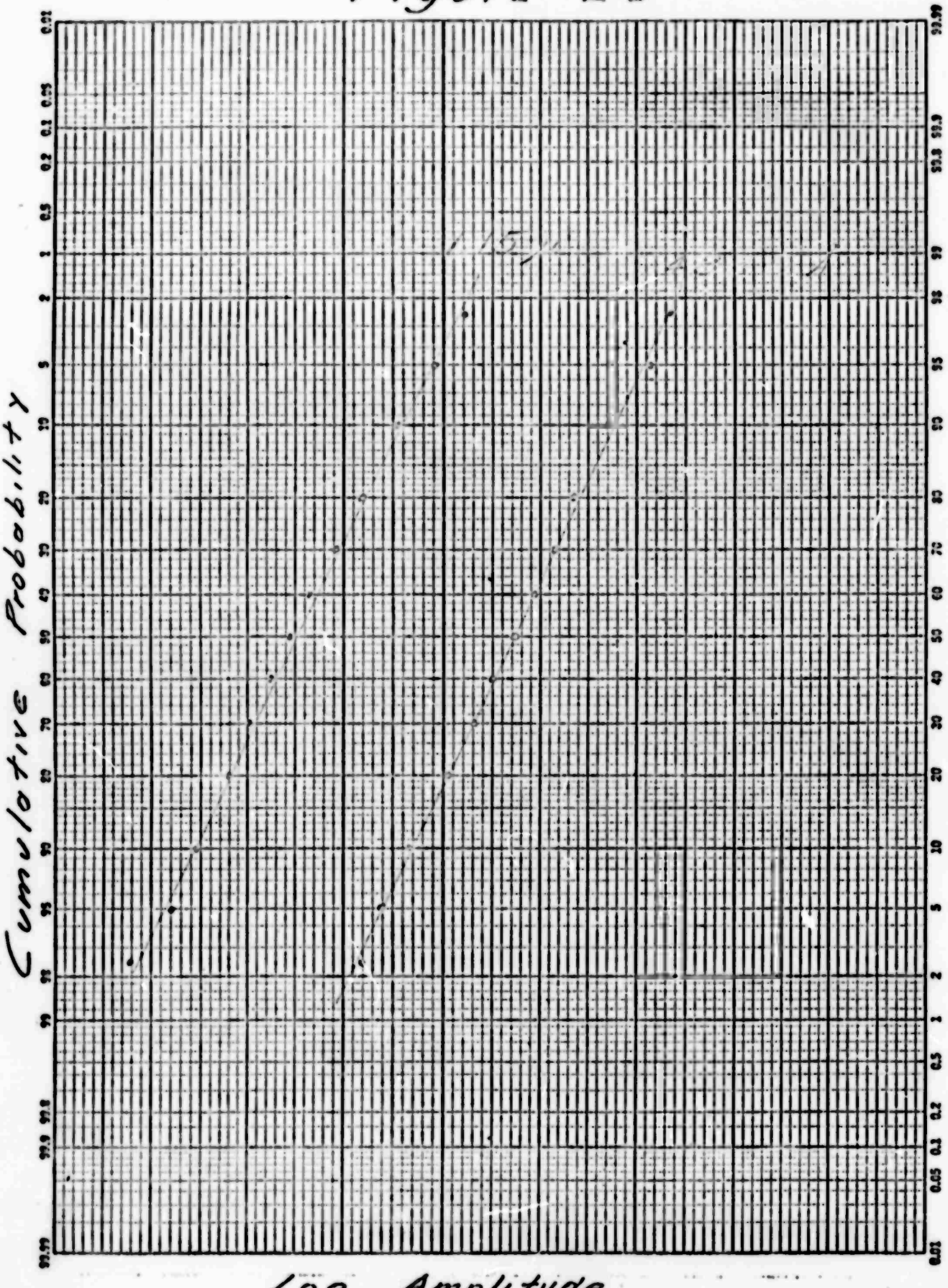

Figure 2a (cont.)

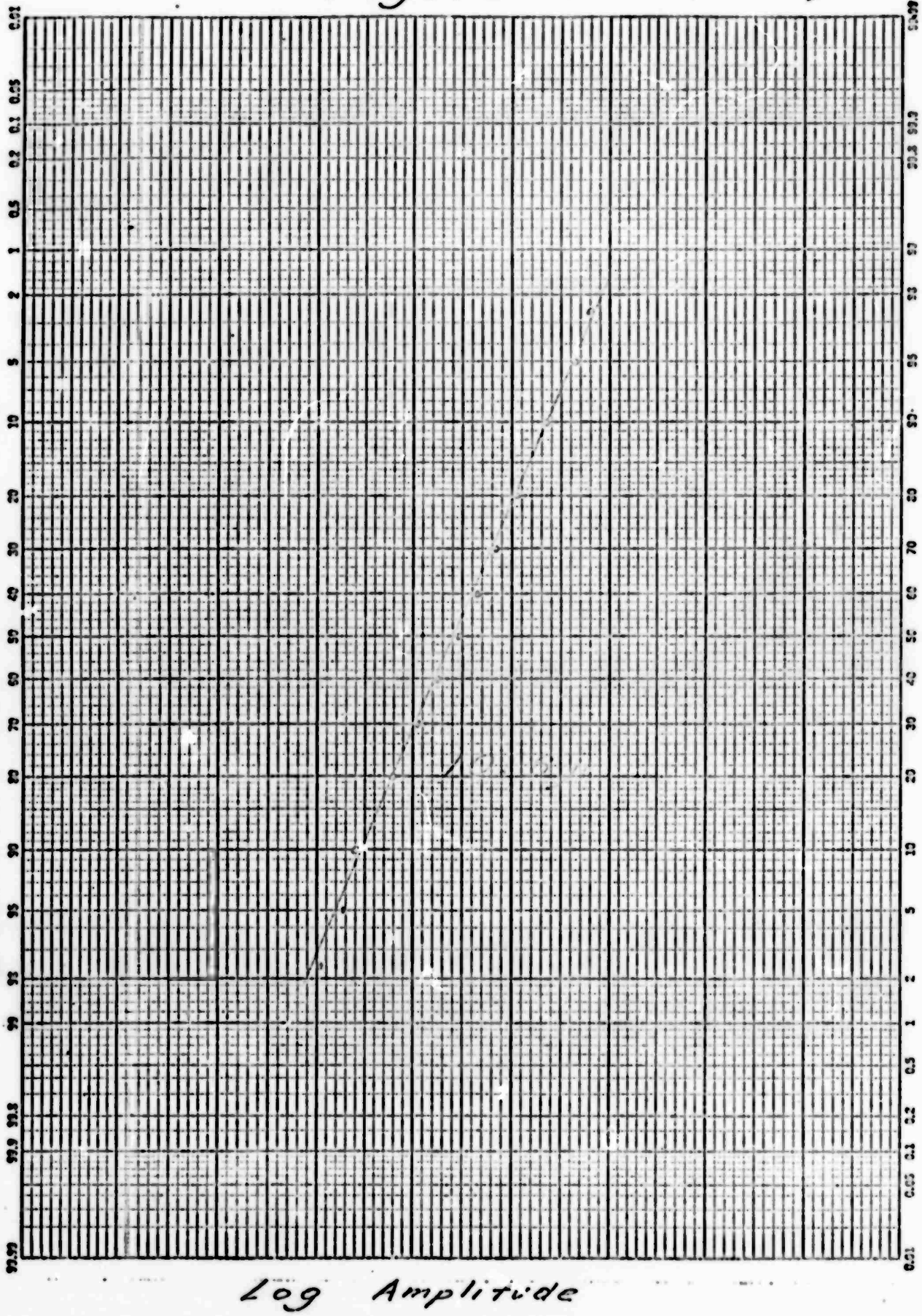

Figure 2b

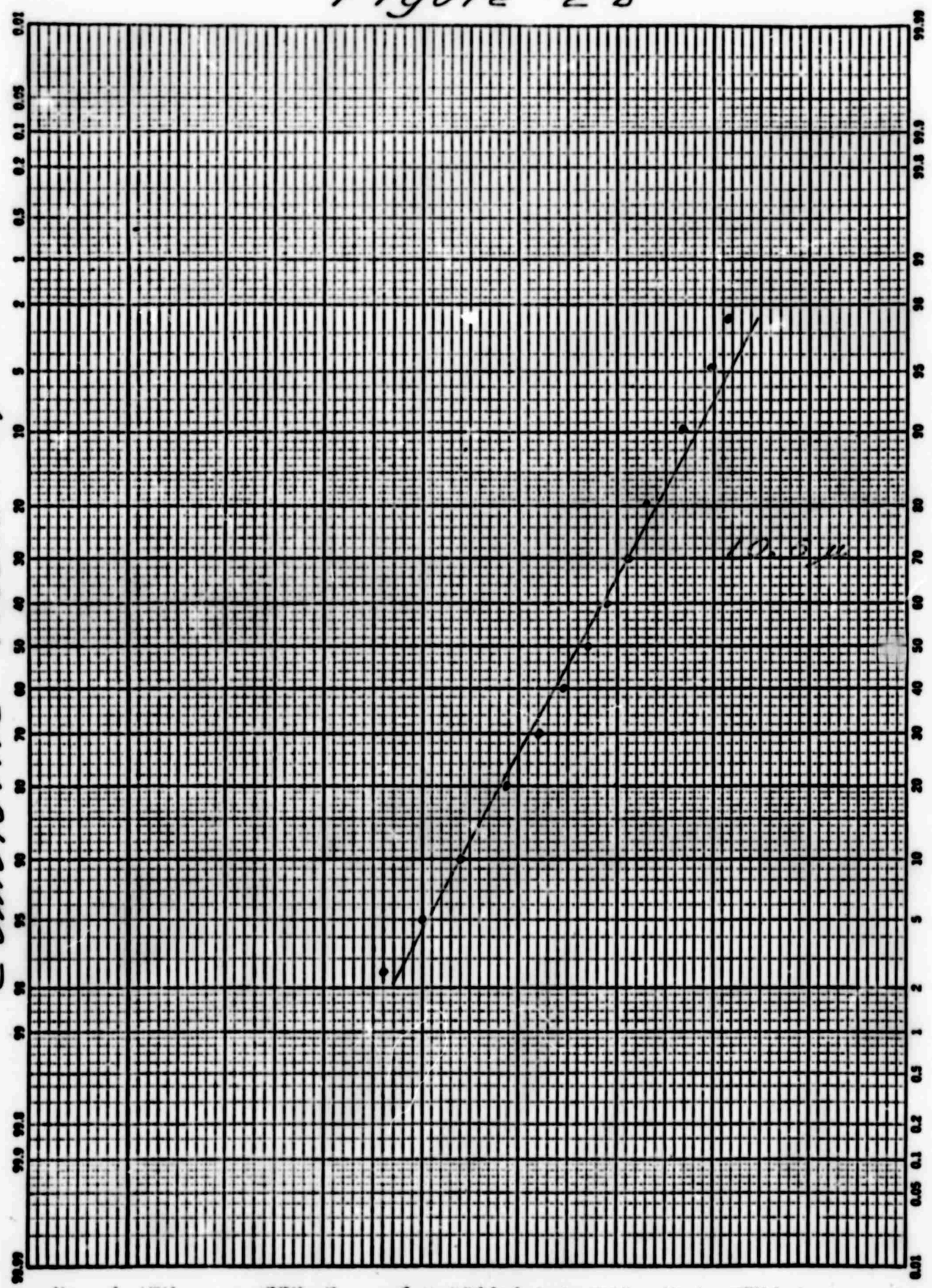

Figure 3a - 1880 Å

NOT REPRODUCIBLE

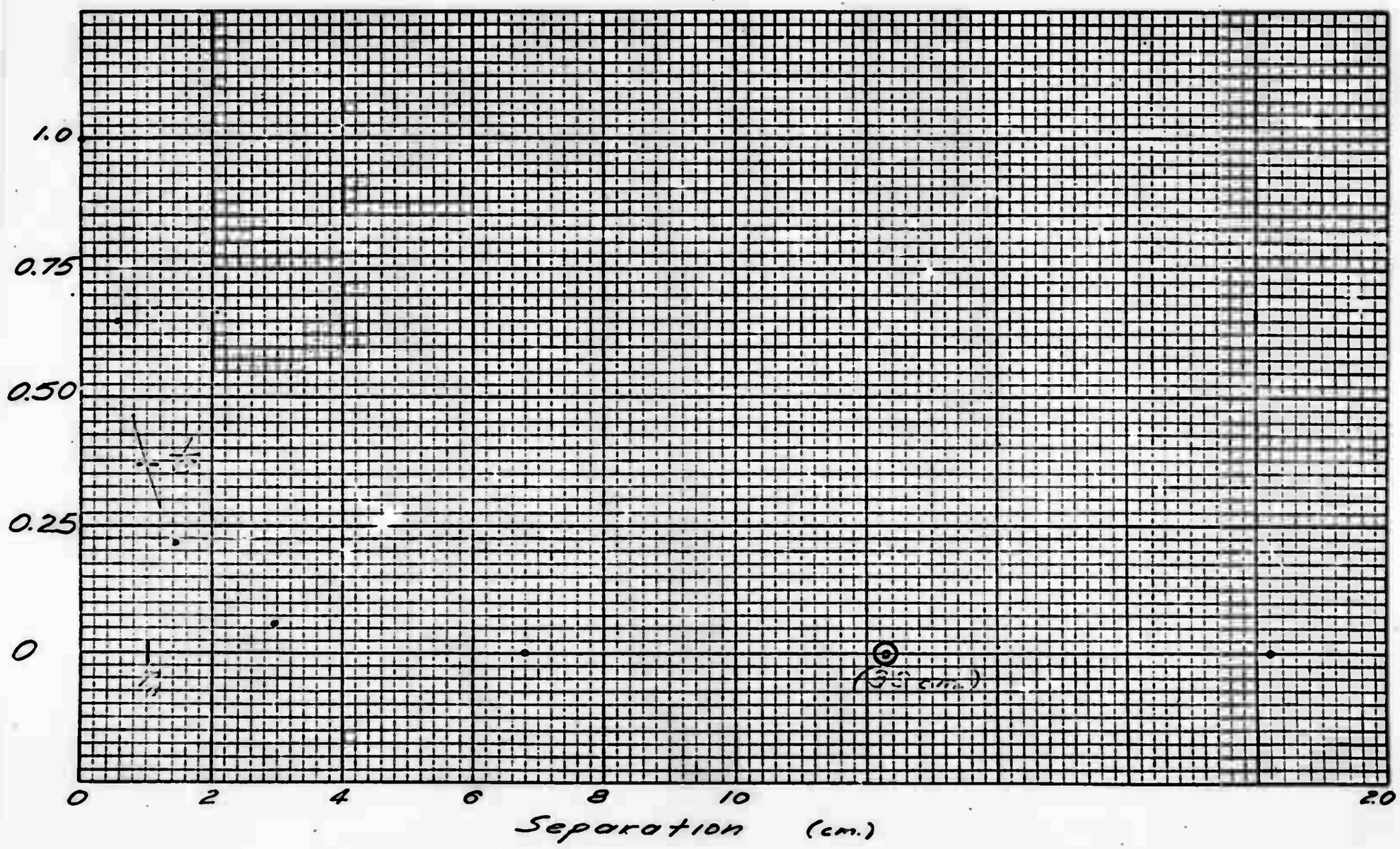

Figure 36 - 1.15μ.

Covariance
Variance

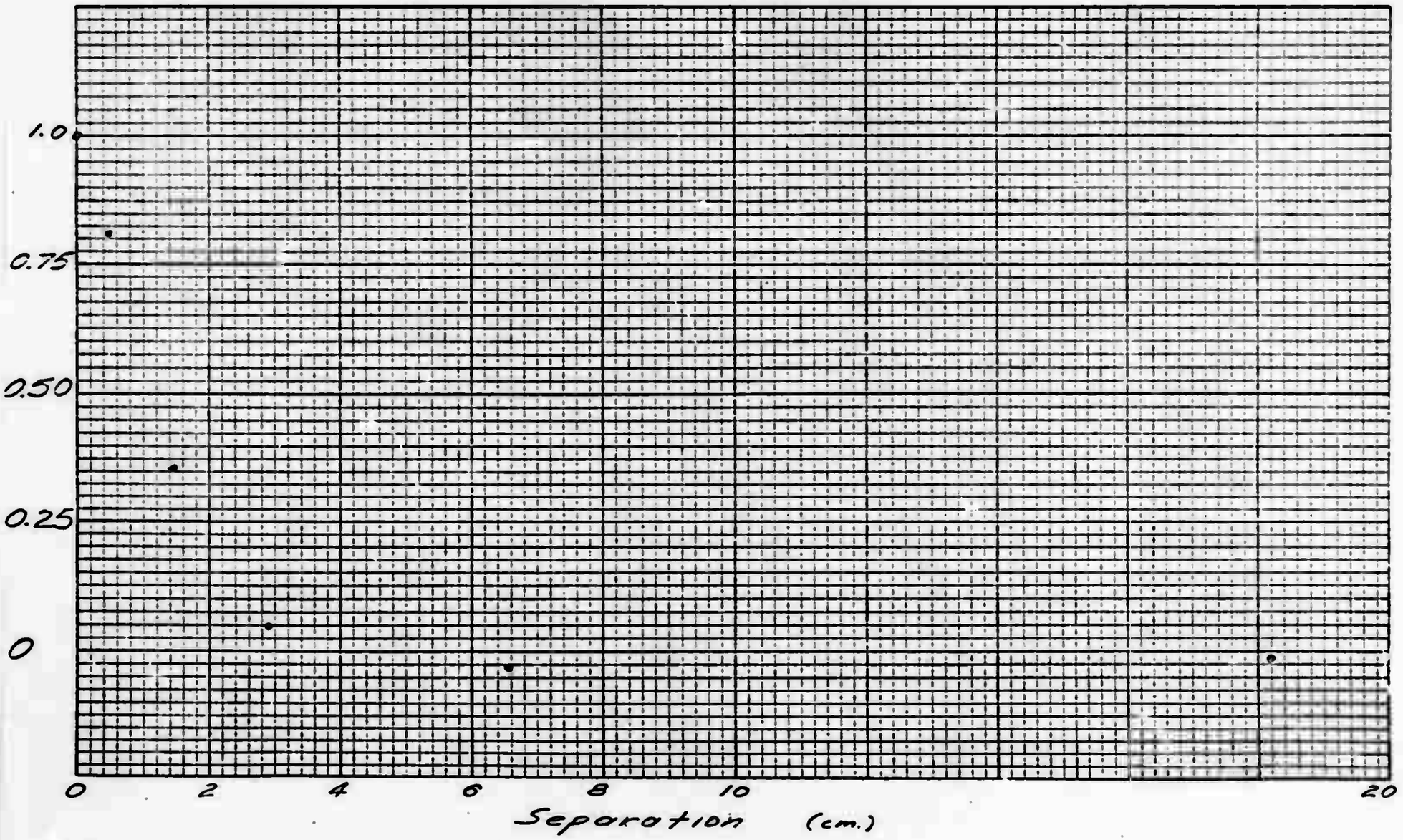

Figure 3c - 10.5μ

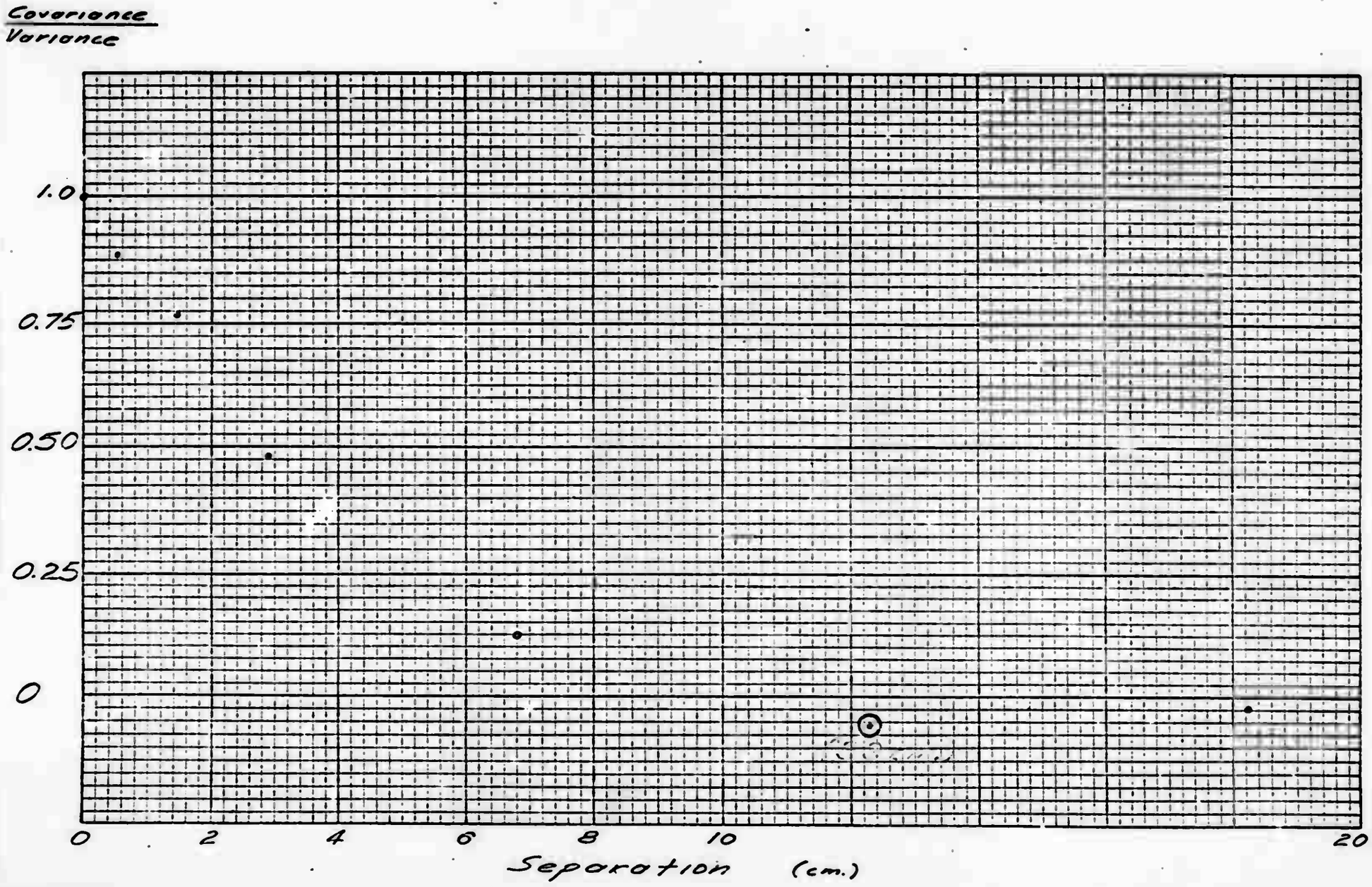

Figure 40-4e20i

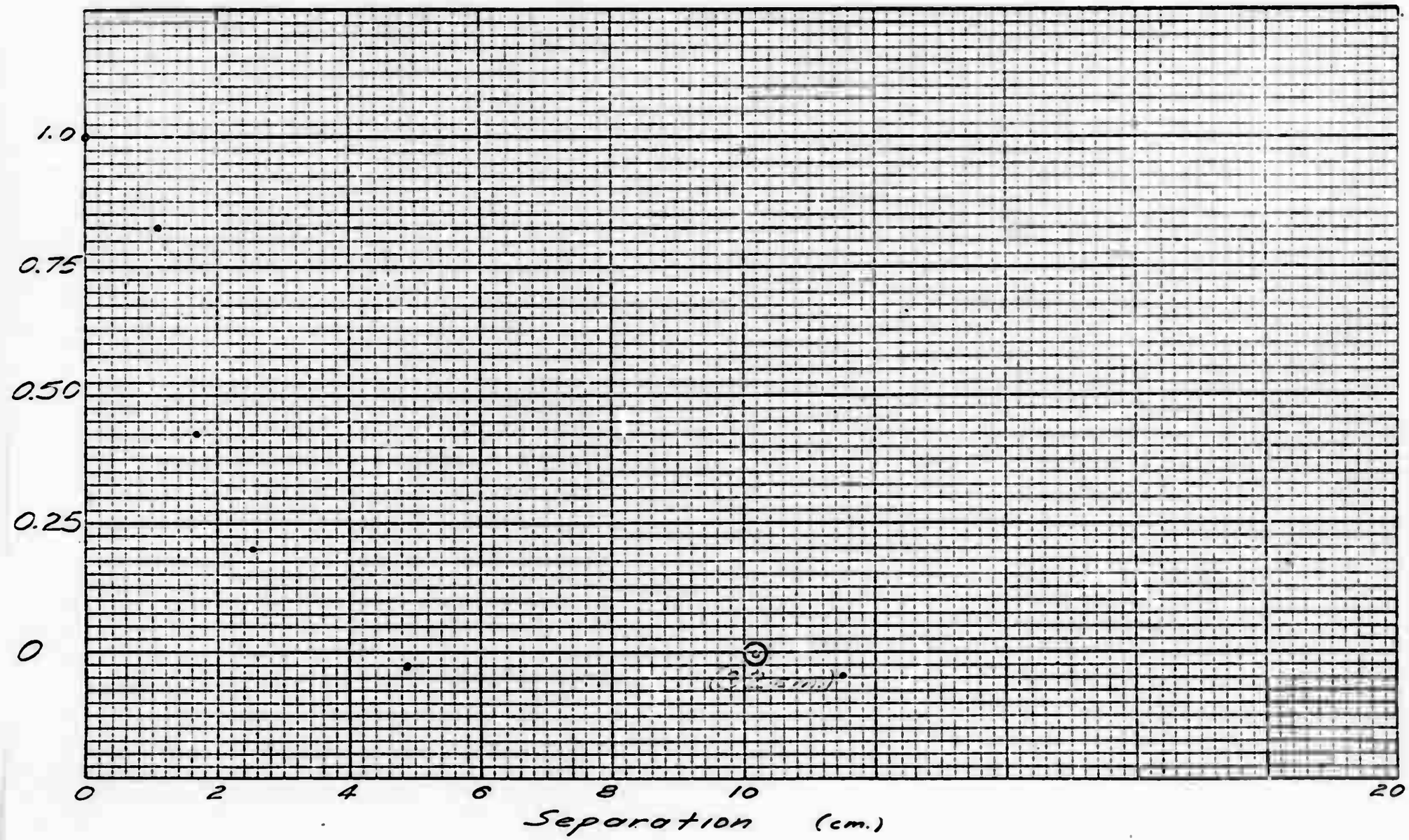

Figure 46 - 1.15 μ

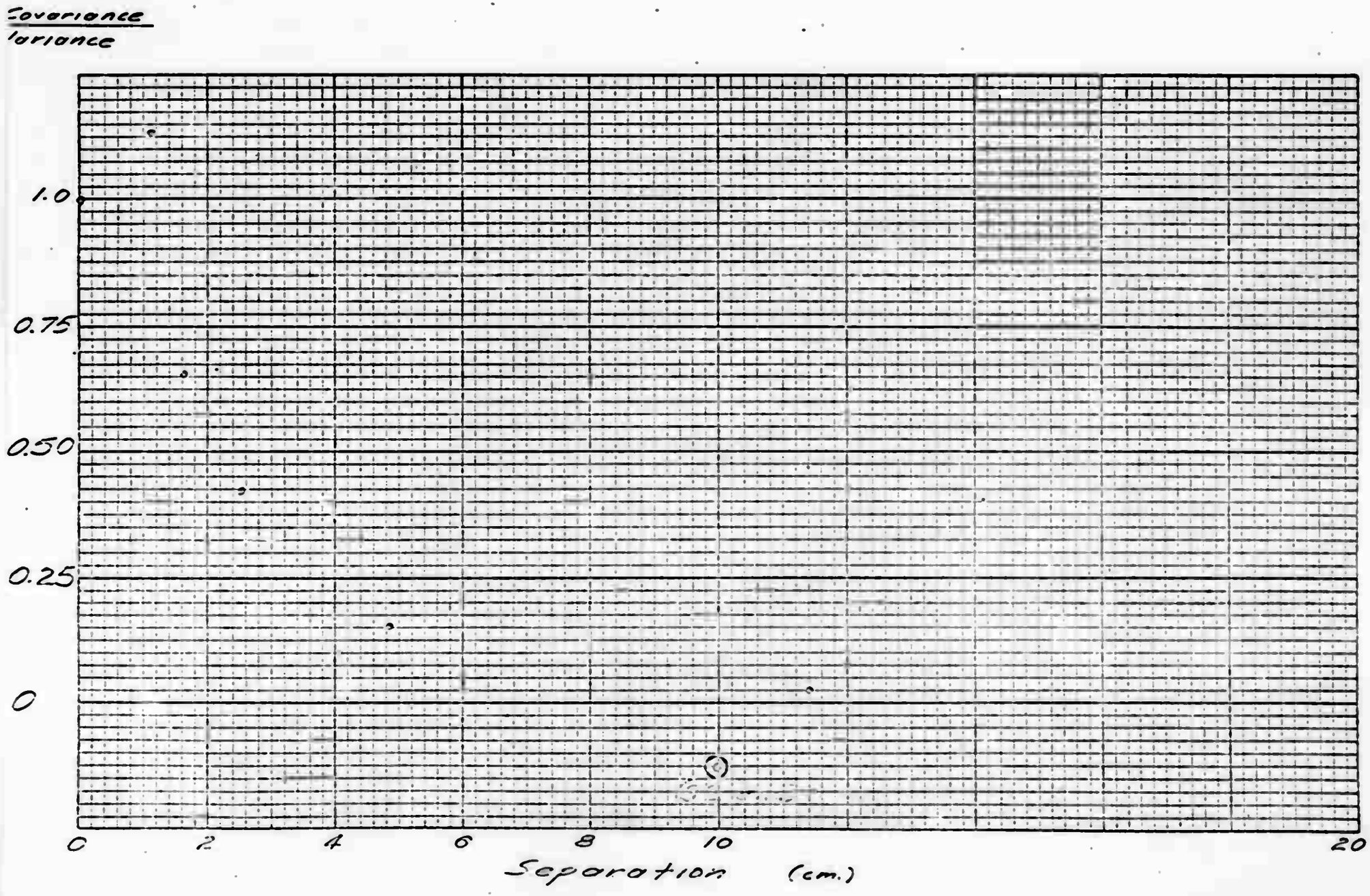

Figure 4c - 10.6 μ

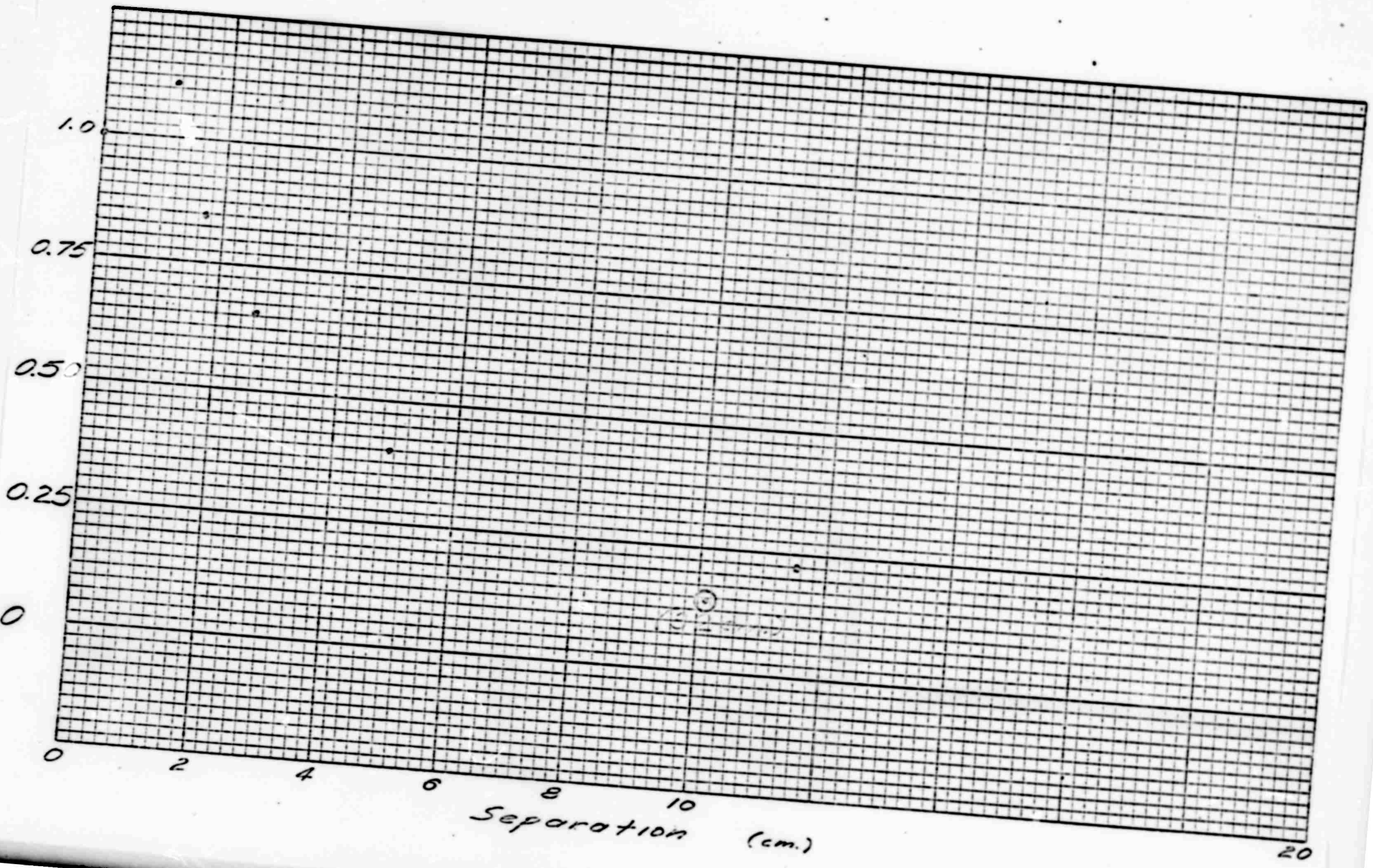

Figure 5a - 4880 Å

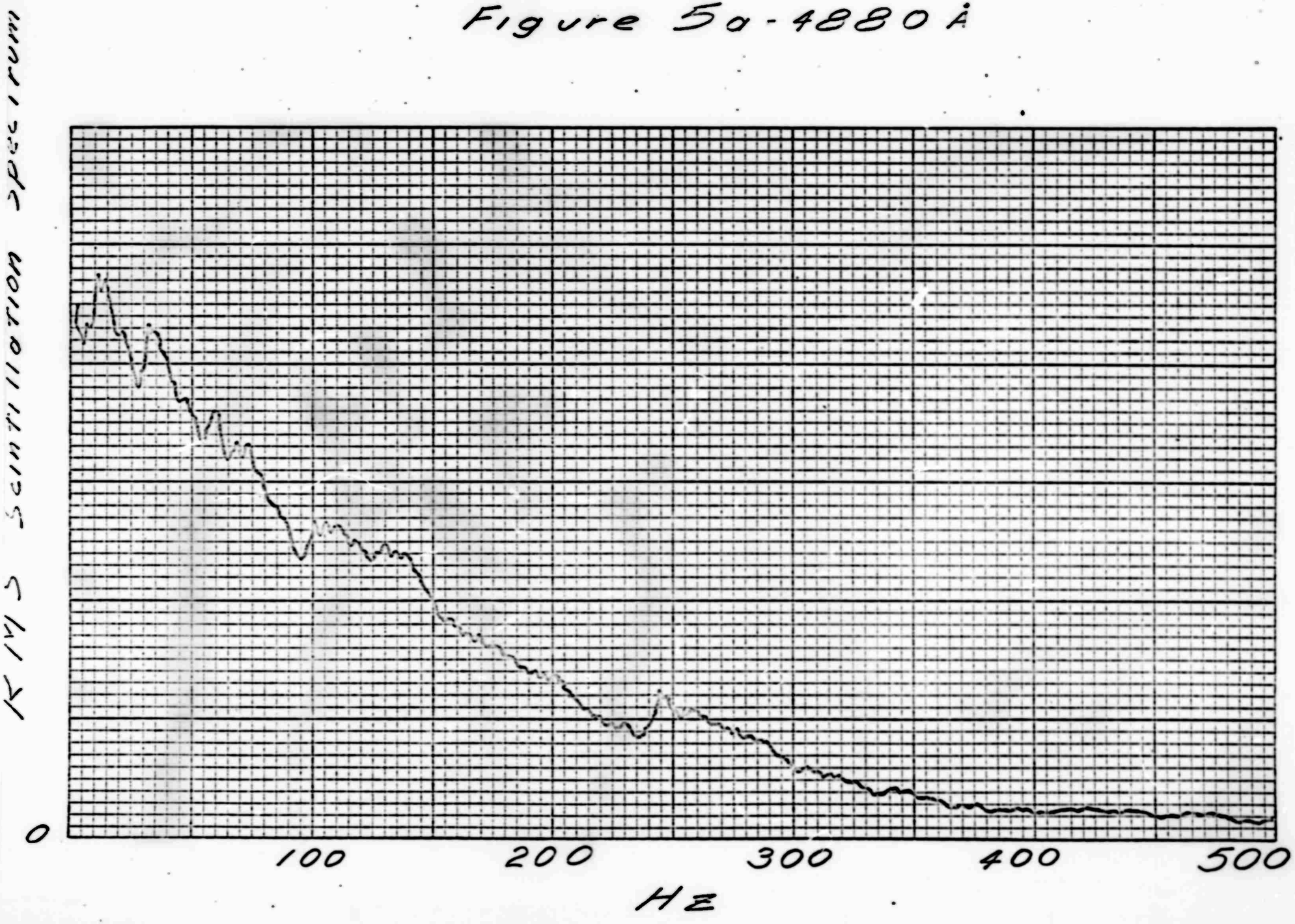

Figure 56 - 1.15 μ

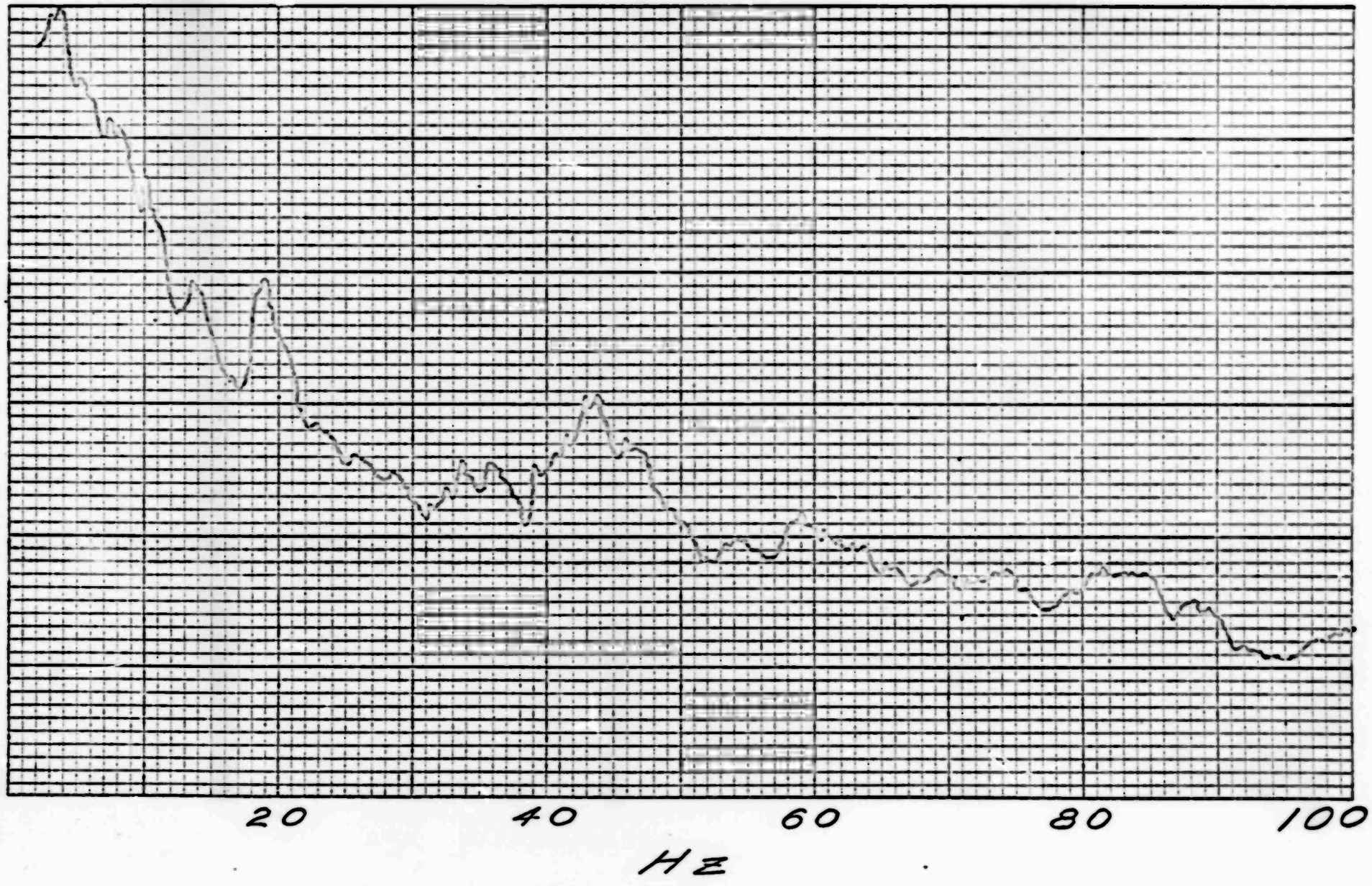

Figure 5c - 10.6μ

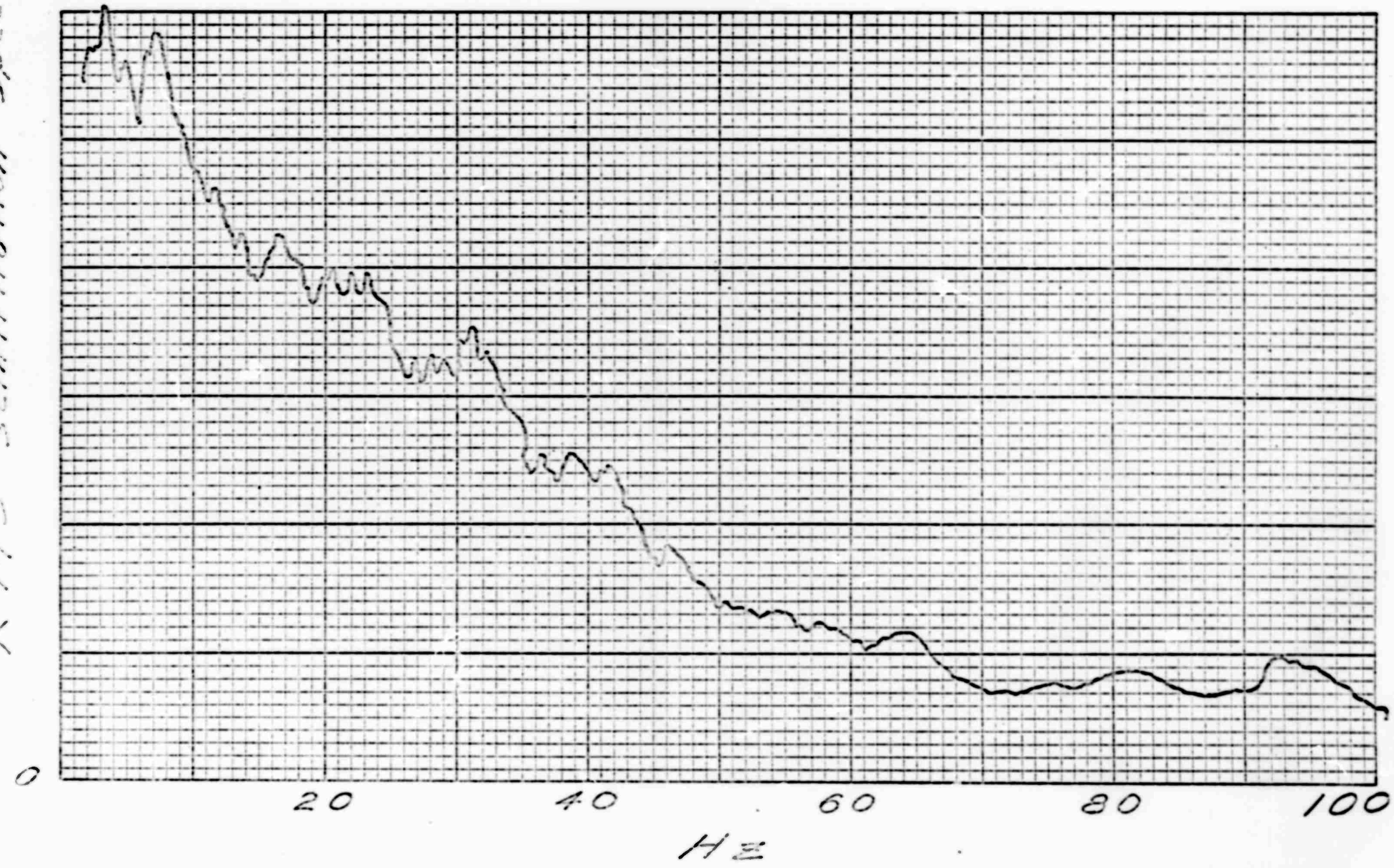

Figure 6a

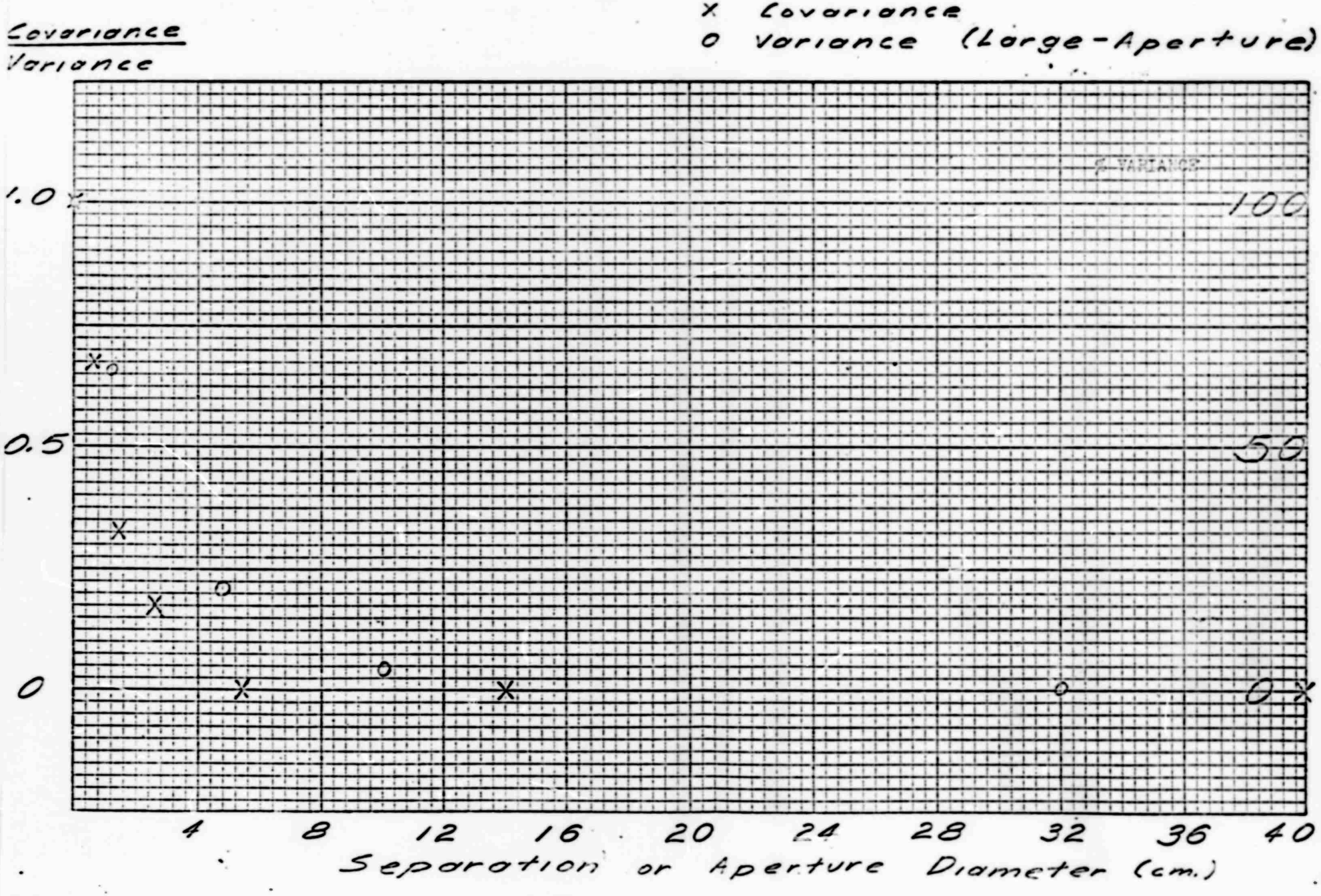
x Covariance
o Variance (Large-Aperture)
Covariance / Variance
% VARIANCE
1.0
0.5
0
100
50
0
4
8
12
16
20
24
28
32
36
40
Separation or Aperture Diameter (cm.)

Figure 6b

× Covariance
o Variance (Large-Aperture)

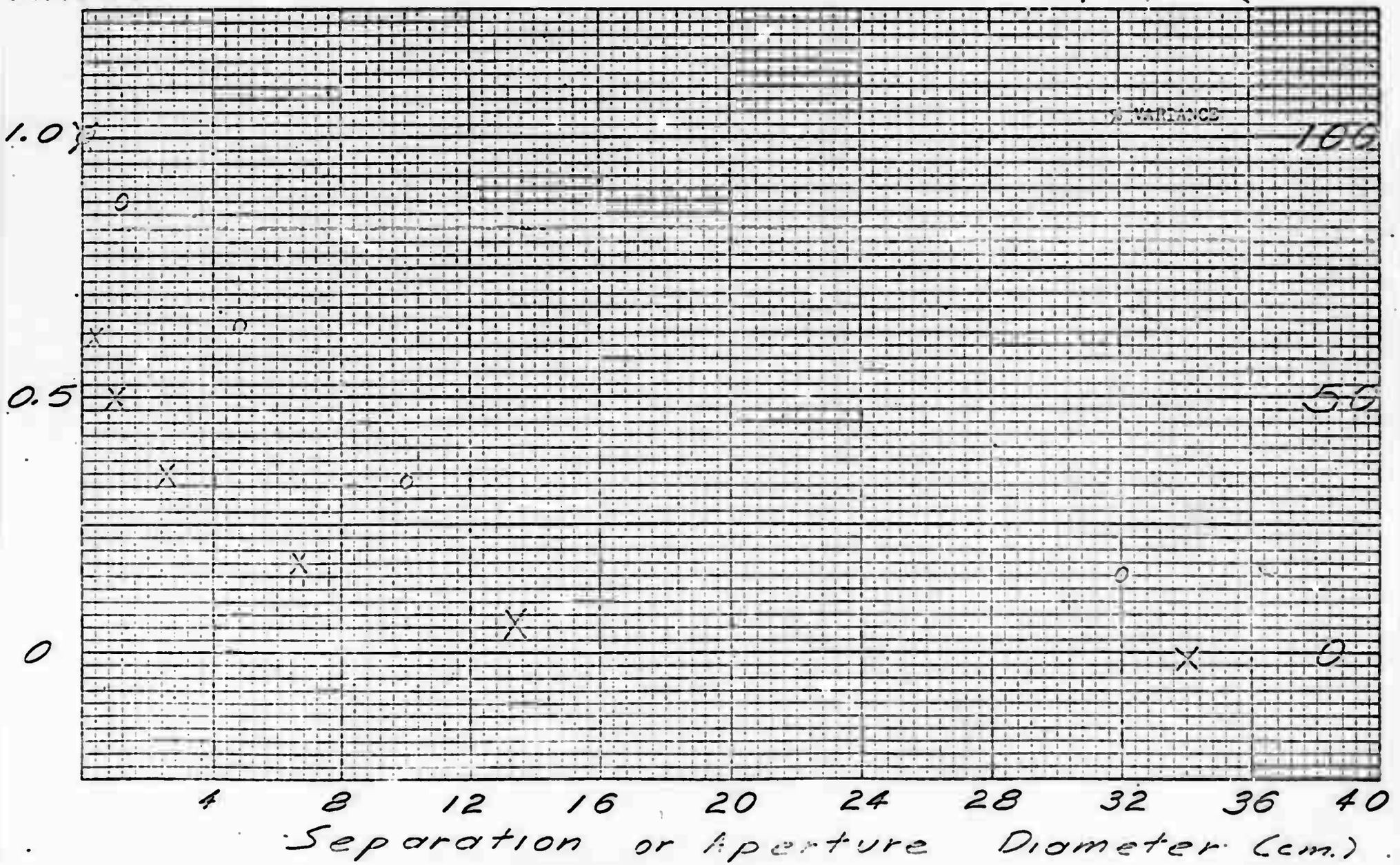

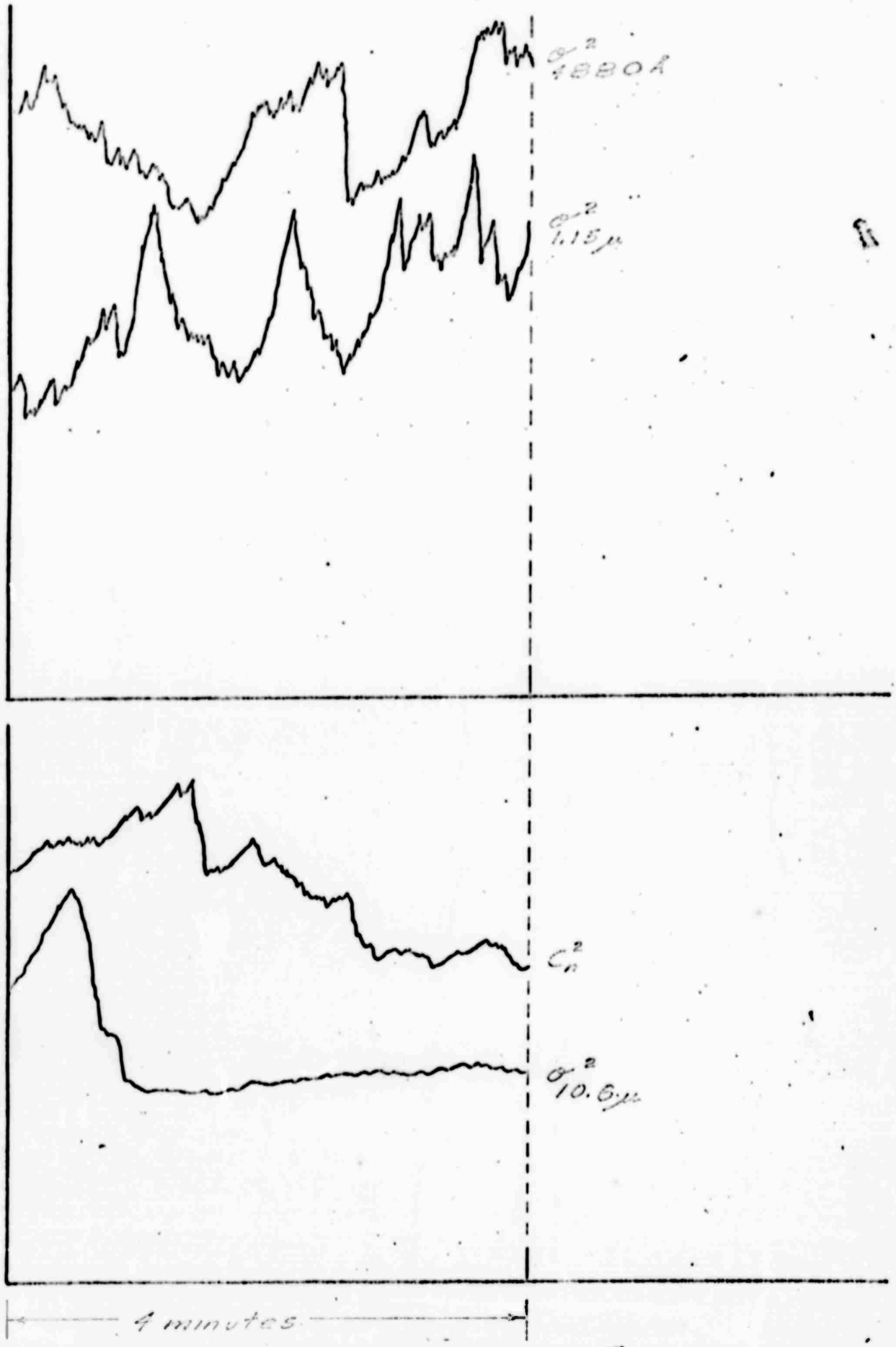

Figure 7.

Figure 8

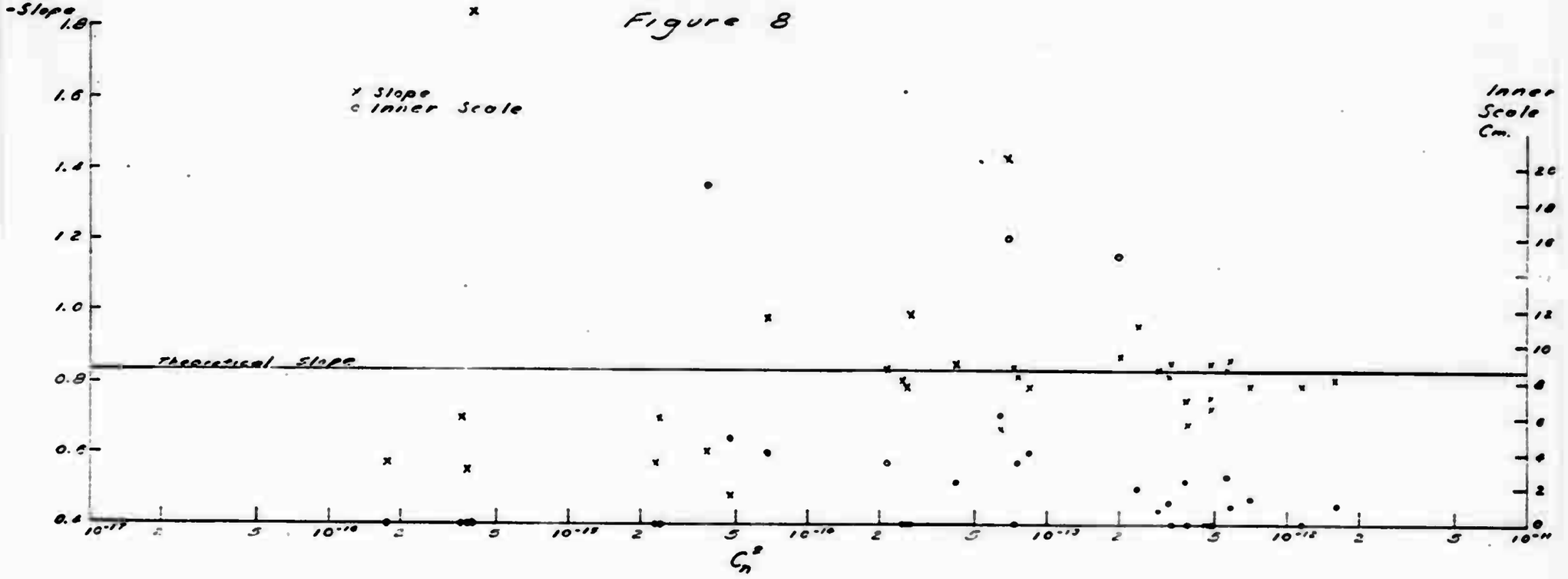
-Slope
1.8
1.6
1.4
1.2
1.0
0.8
0.6
0.4
× Slope
○ Inner Scale
Theoretical Slope
Inner Scale Cm.
20
18
16
14
12
10
8
6
4
2
0
10⁻¹⁷
2
5
10⁻¹⁶
2
5
10⁻¹⁵
2
5
10⁻¹⁴
2
5
10⁻¹³
2
5
10⁻¹²
2
5
10⁻¹¹
C_n^2

Figure 9

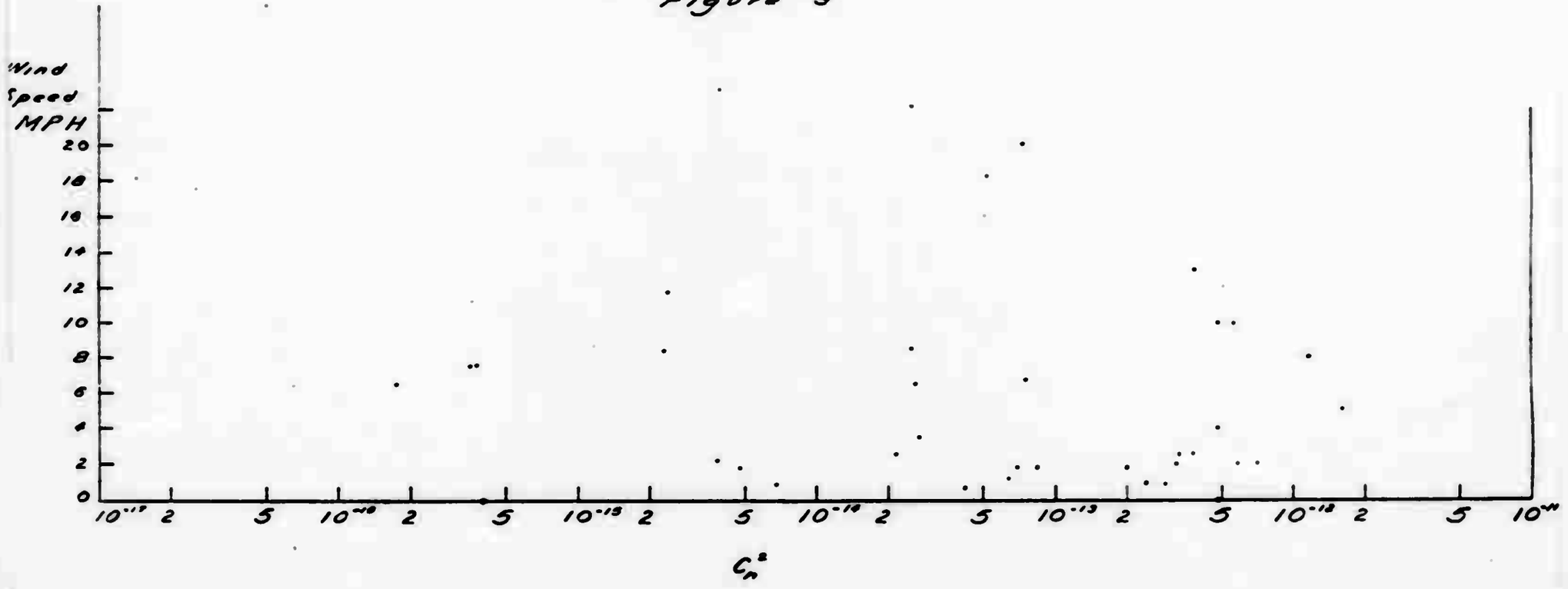
Wind Speed MPH
20
18
16
14
12
10
8
6
4
2
0
10^{-11} 2 5 10^{-10} 2 5 10^{-9} 2 5 10^{-8} 2 5 10^{-7} 2 5 10^{-6} 2 5 10^{-5}
C_n^2

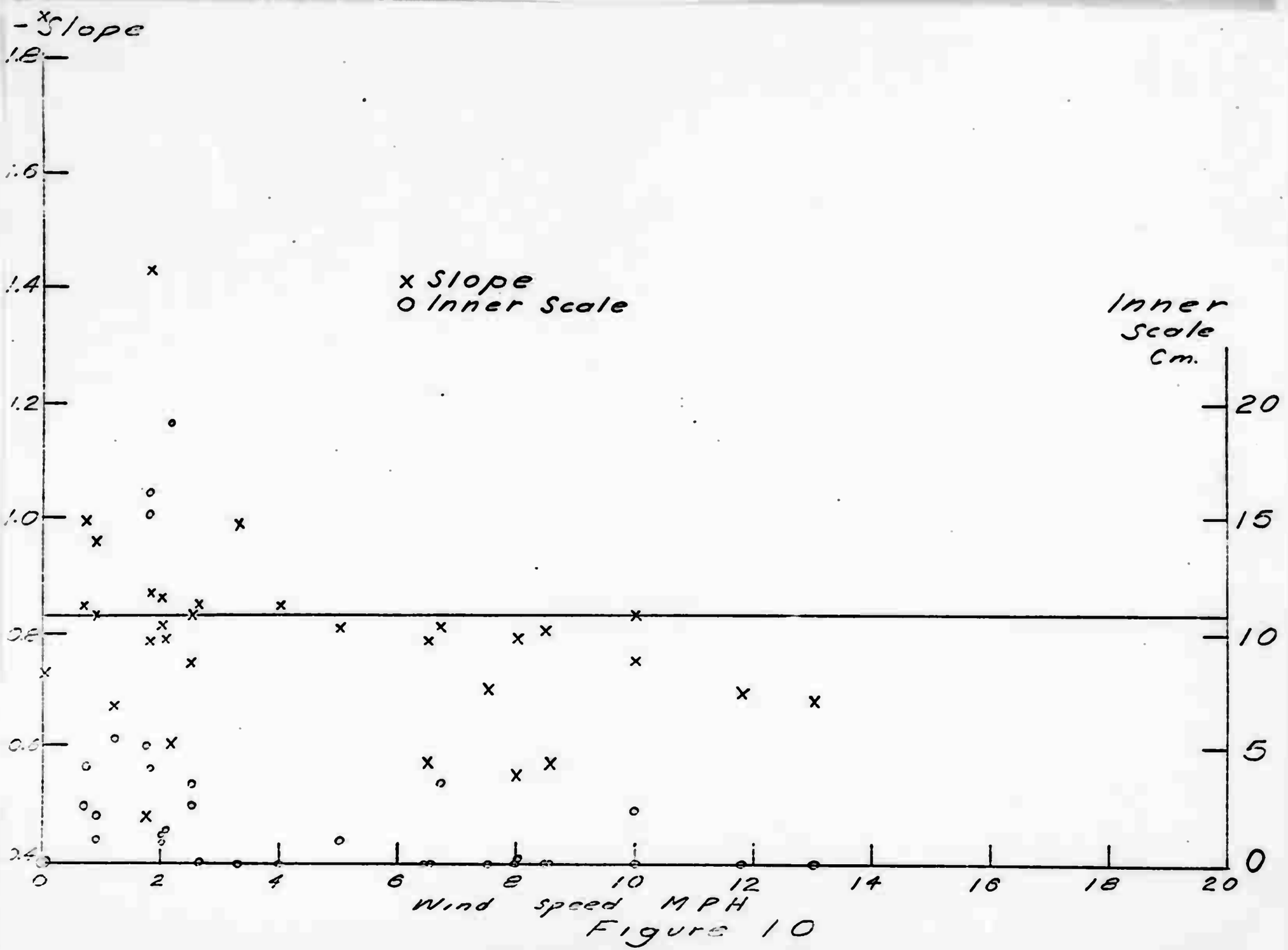
-x Slope
1.8
1.6
1.4
1.2
1.0
0.8
0.6
0.4
x Slope
o Inner Scale
Inner Scale Cm.
20
15
10
5
0
0
2
4
6
8
10
12
14
16
18
20
Wind speed MPH

Figure 10

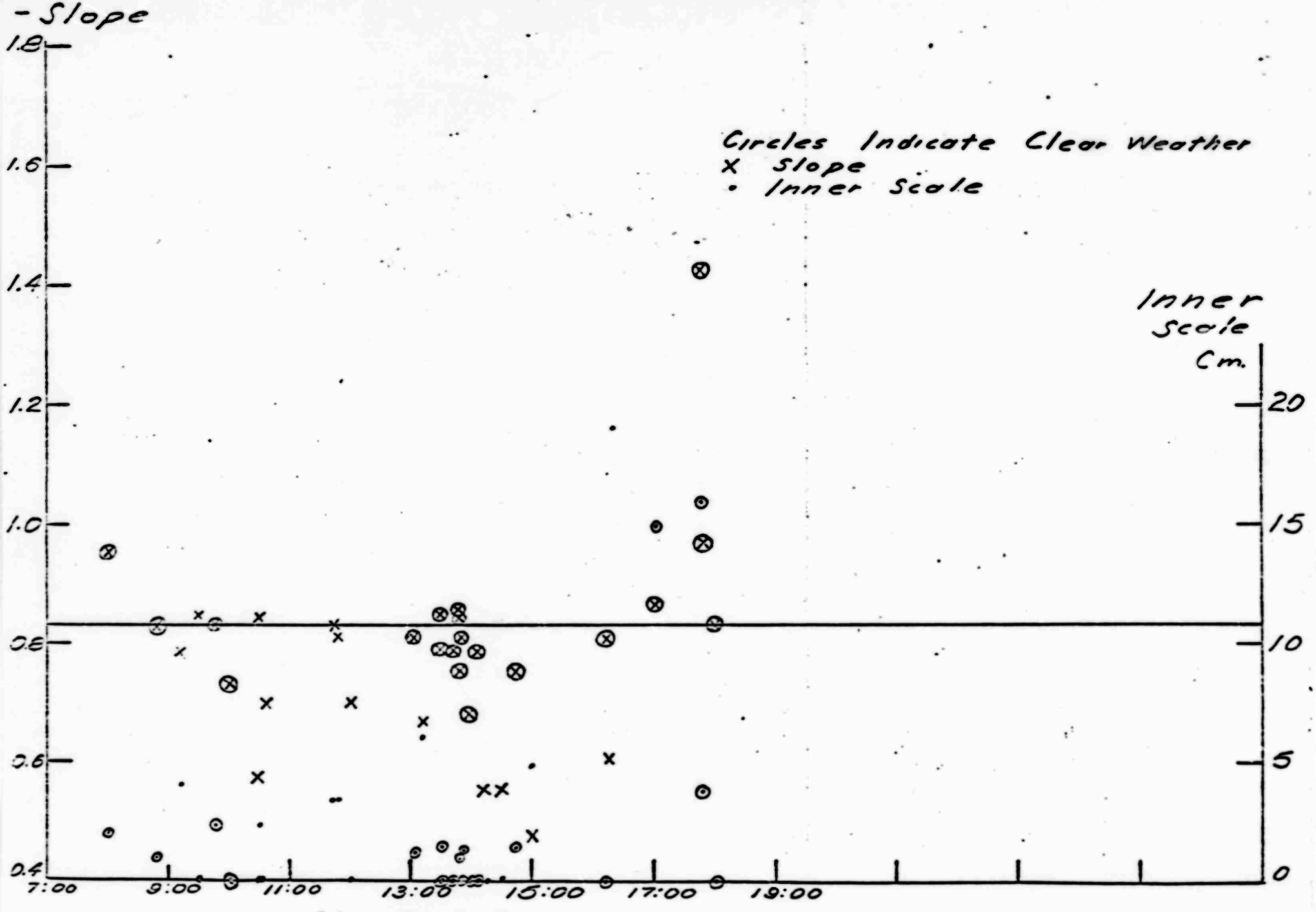
- Slope
1.8
1.6
1.4
1.2
1.0
0.8
0.6
0.4
Circles Indicate Clear Weather
× Slope
• Inner Scale
Inner Scale Cm.
20
15
10
5
0
7:00
9:00
11:00
13:00
15:00
17:00
19:00
Standard time

Figure 11

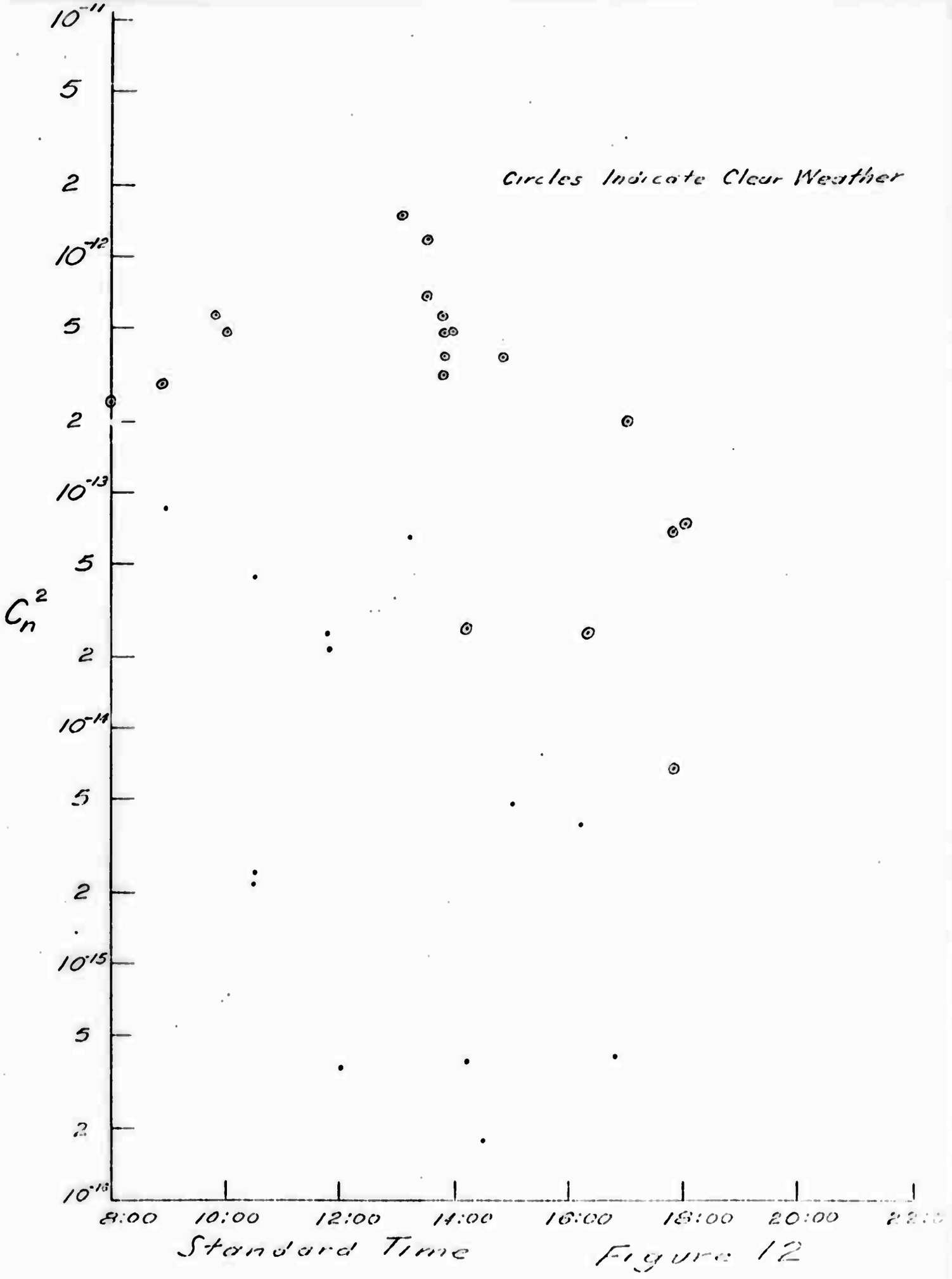
Circles Indicate Clear Weather
10^{-11}
5
2
10^{-12}
5
2
10^{-13}
5
2
10^{-14}
5
2
10^{-15}
5
2
10^{-16}
C_n^2
8:00
10:00
12:00
14:00
16:00
18:00
20:00
Standard Time

Figure 12

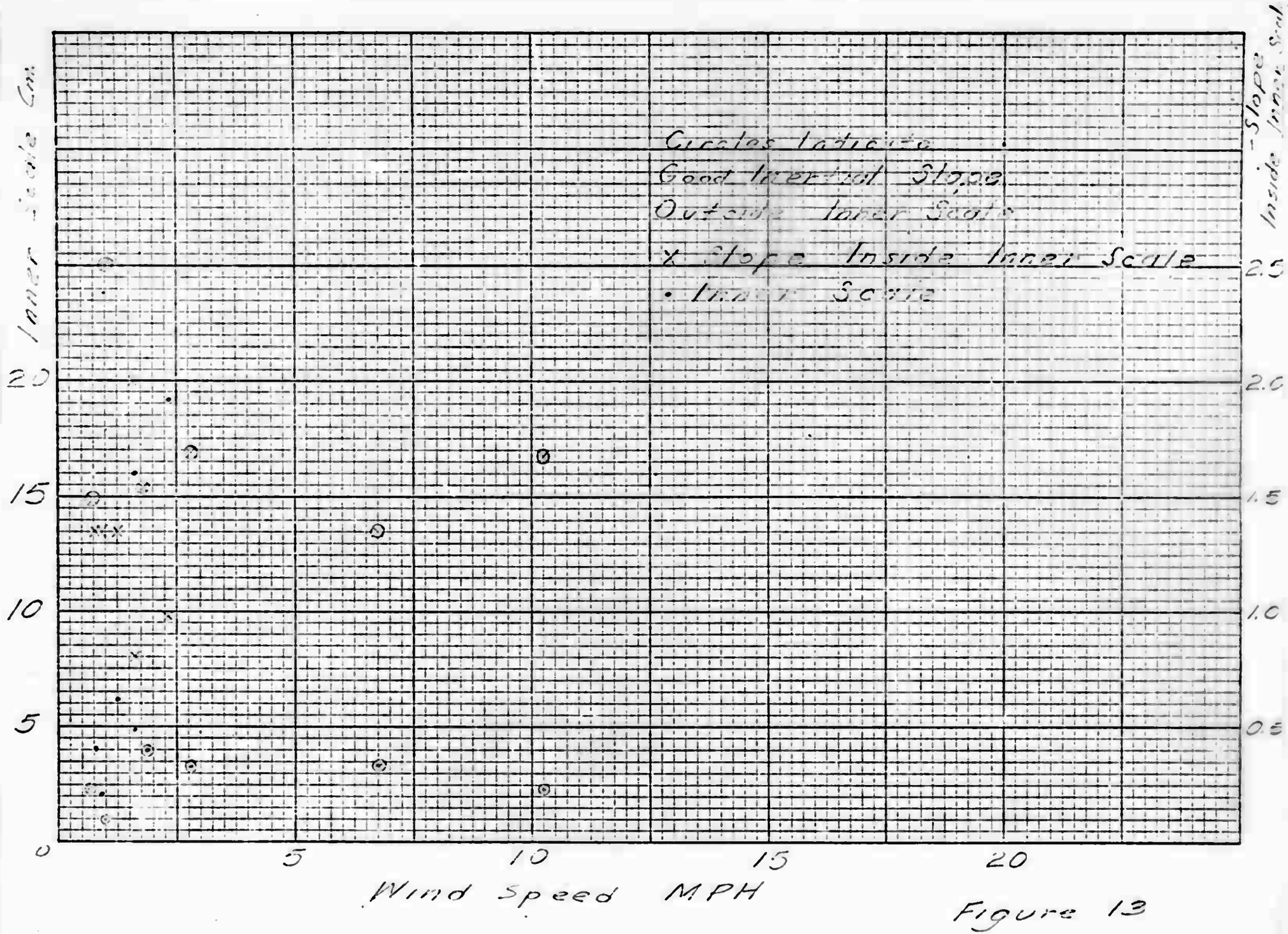
Circular Lattice
Good Interval Slope
Outside Inner Scale
x Slope Inside Inner Scale
• Inner Scale
Inner Scale Cm.
20
15
10
5
0
5
10
15
20
Wind Speed MPH
Inside Inner Scale Slope
2.5
2.0
1.5
1.0
0.5

Figure 13

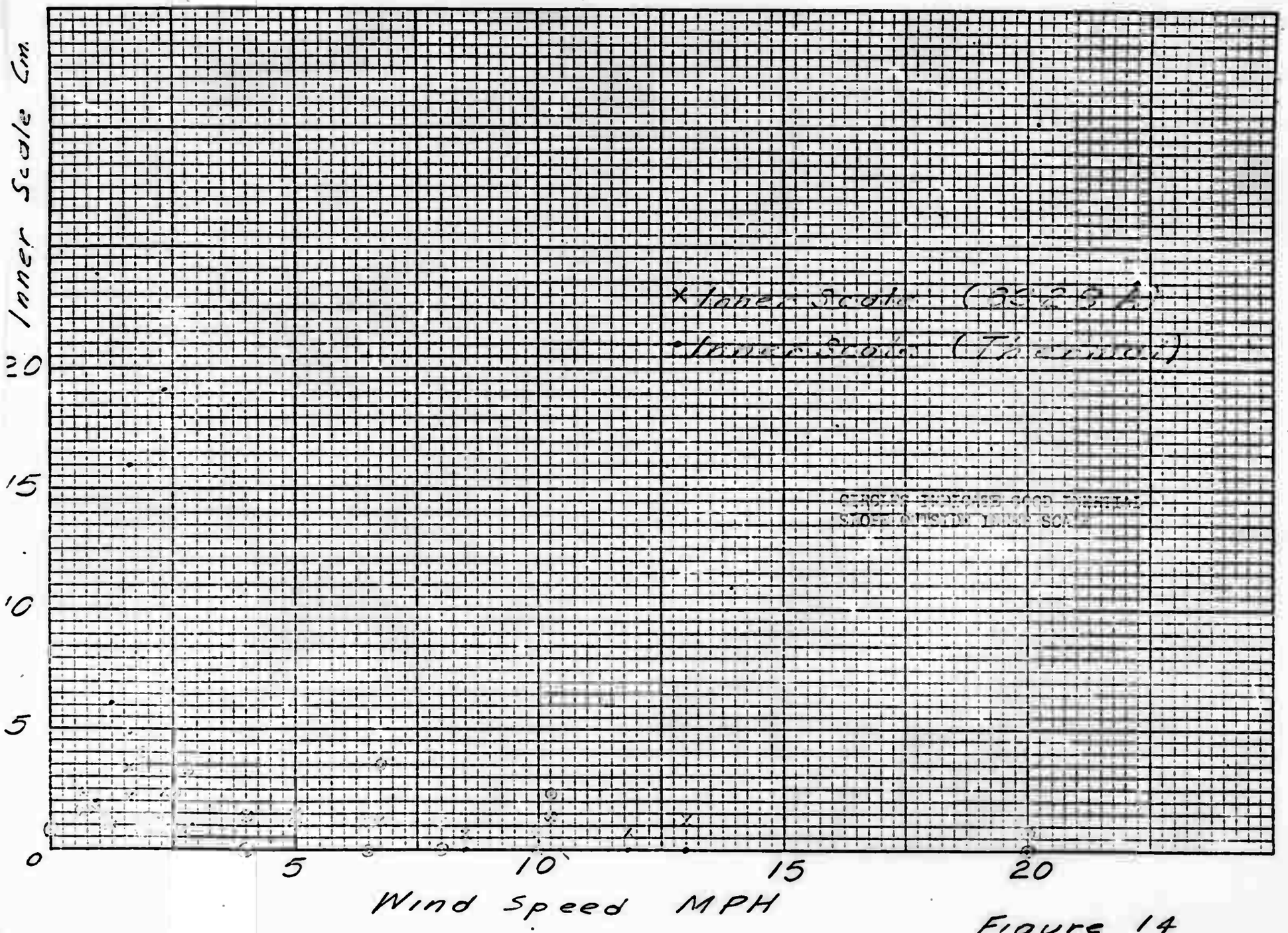

Figure 14

Circles Indicate
Good Inertial Slope
Outside Inner Scale

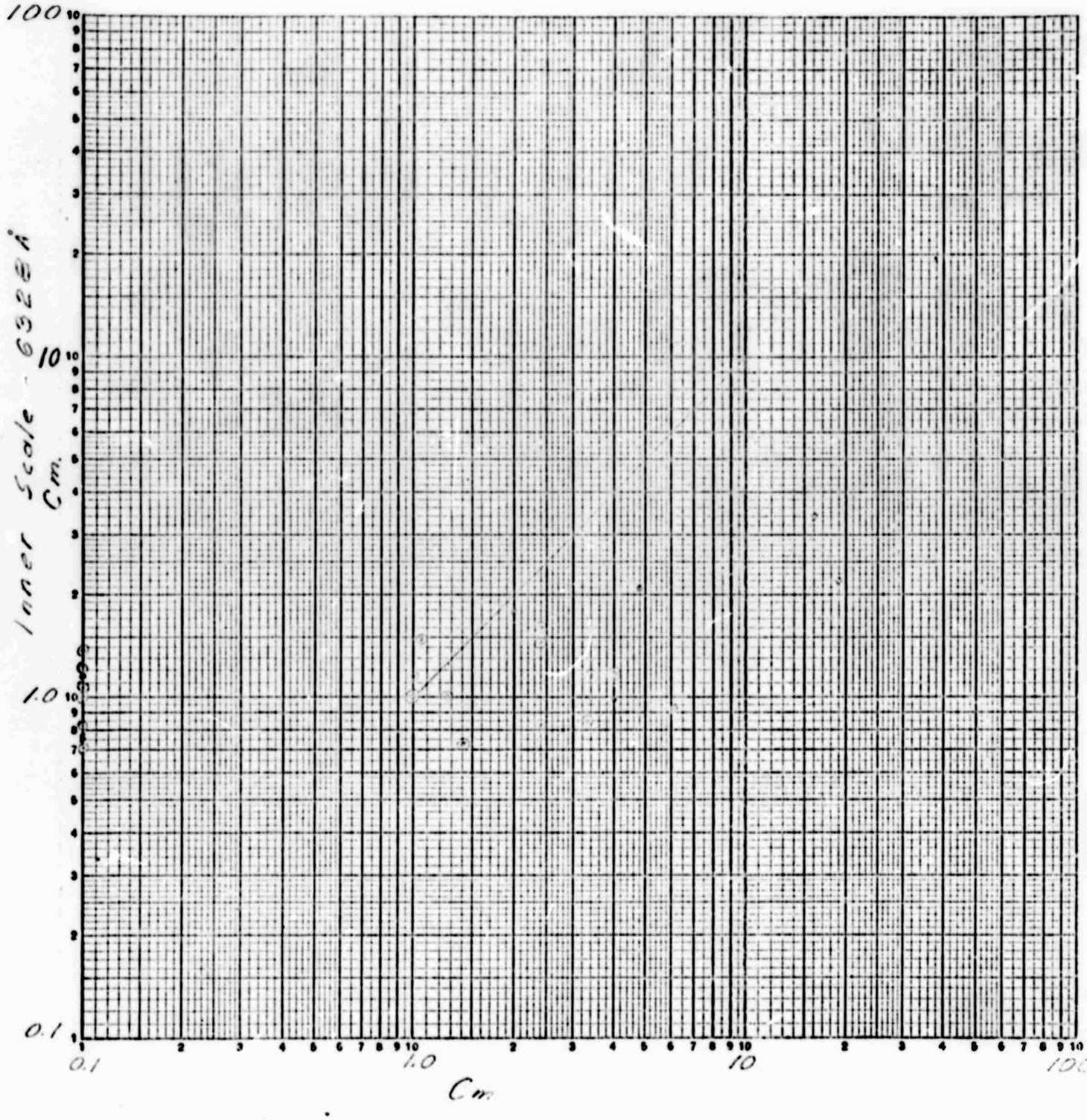

Inner Scale—Thermal

Figure 15

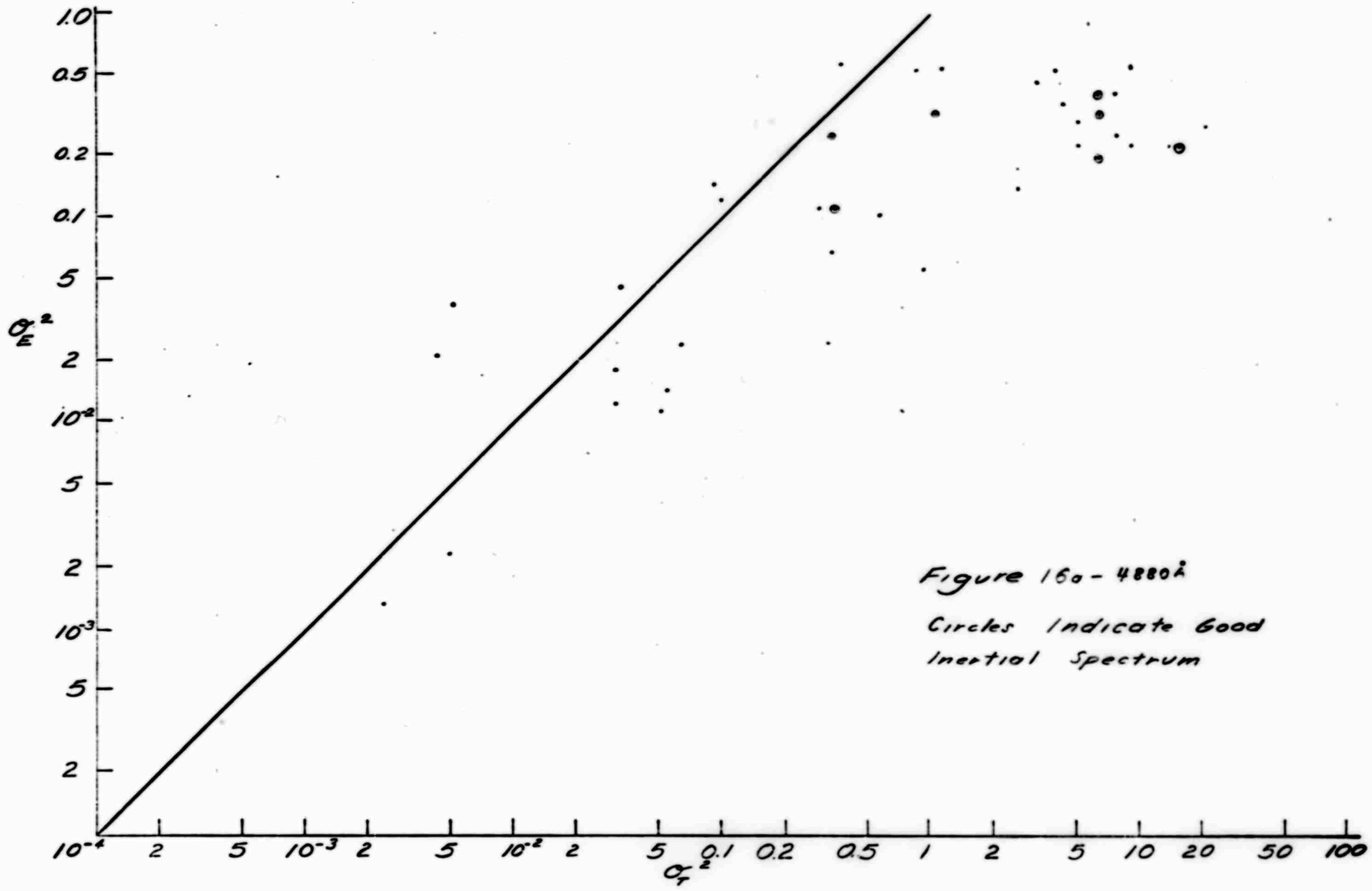

Figure 16a - 4880Å

Circles Indicate Good Inertial Spectrum

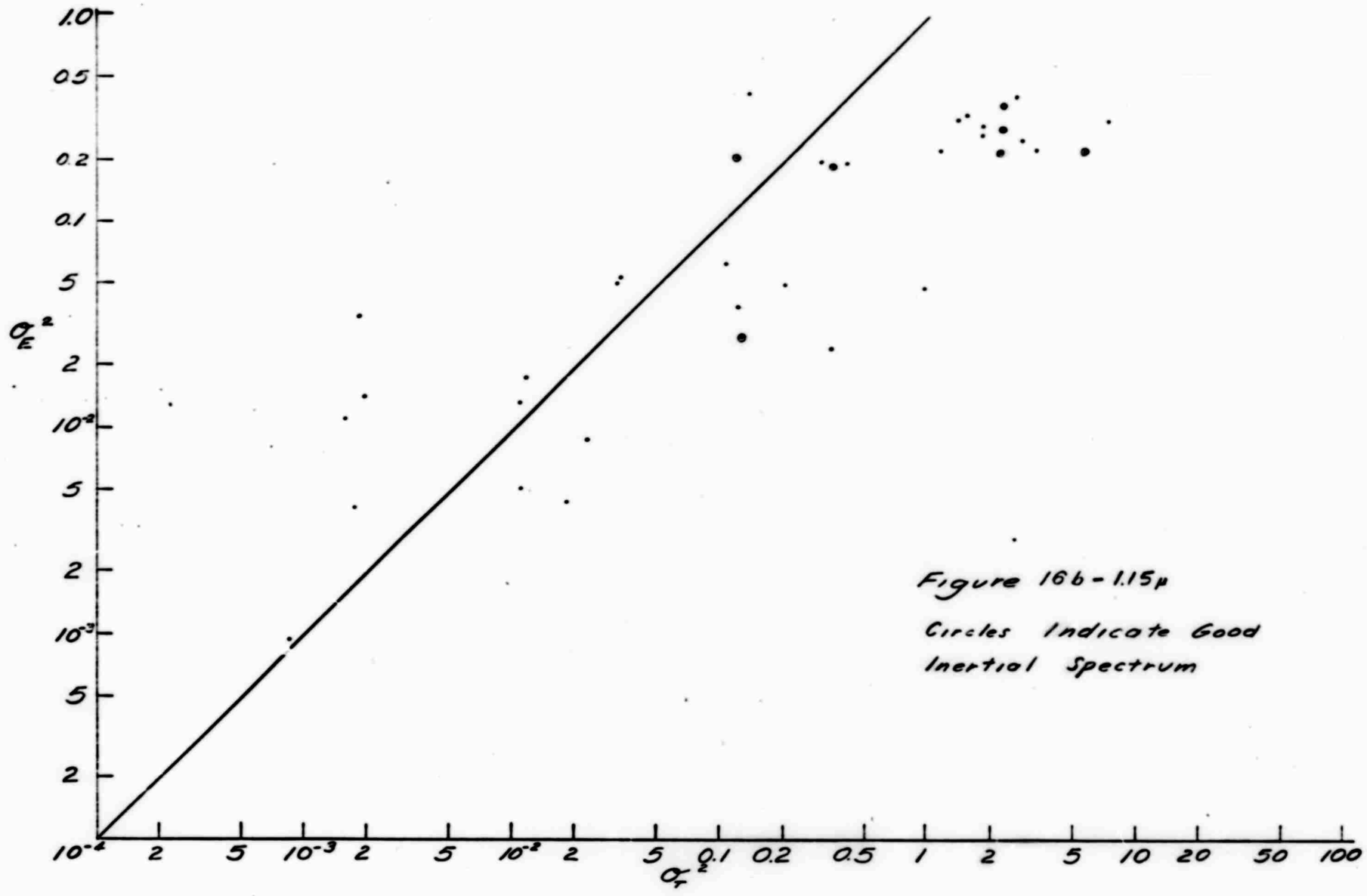

Figure 16b - 1.15μ

Circles Indicate Good Inertial Spectrum

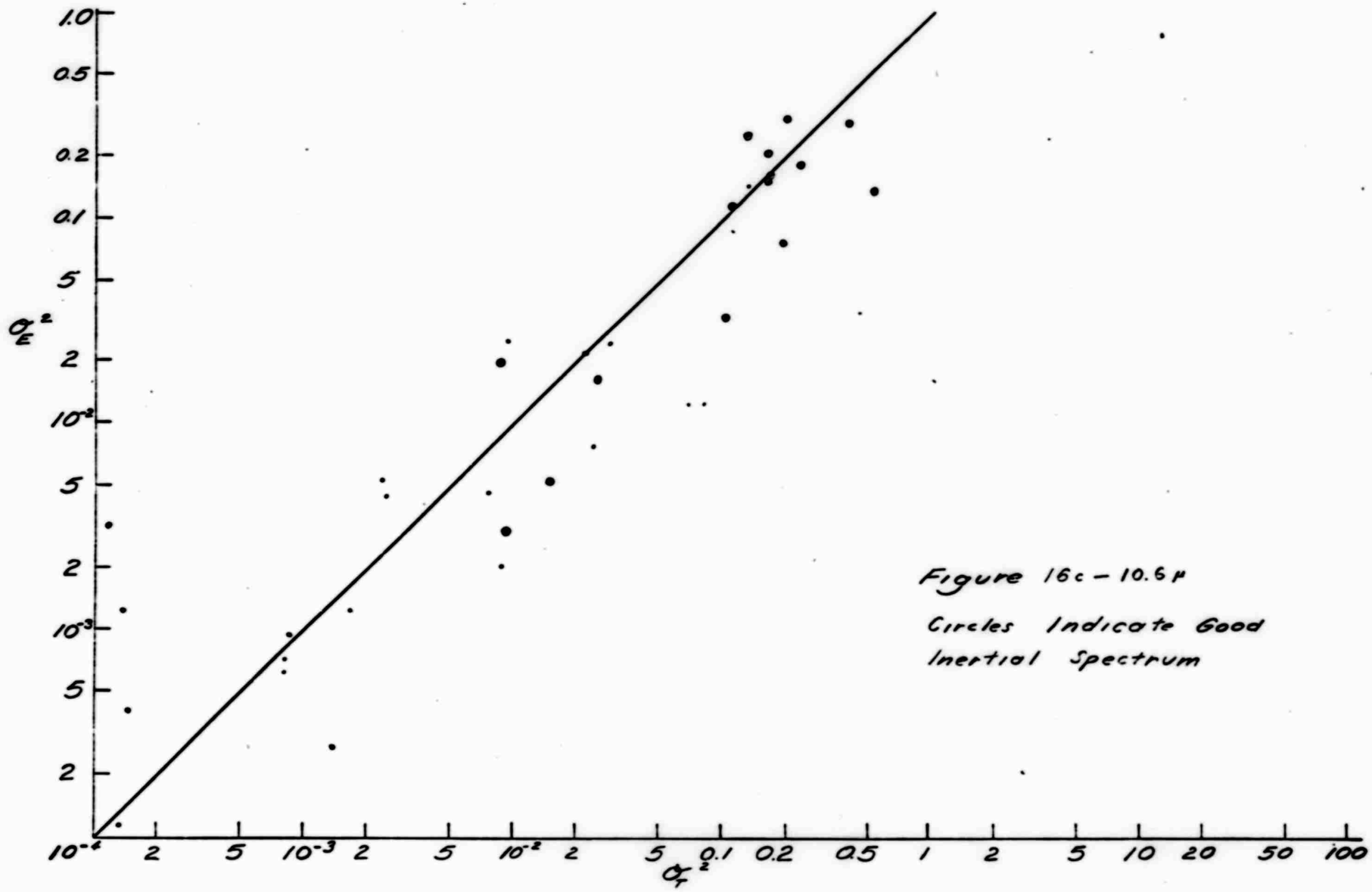

Figure 16c – 10.6 μ

Circles Indicate Good Inertial Spectrum

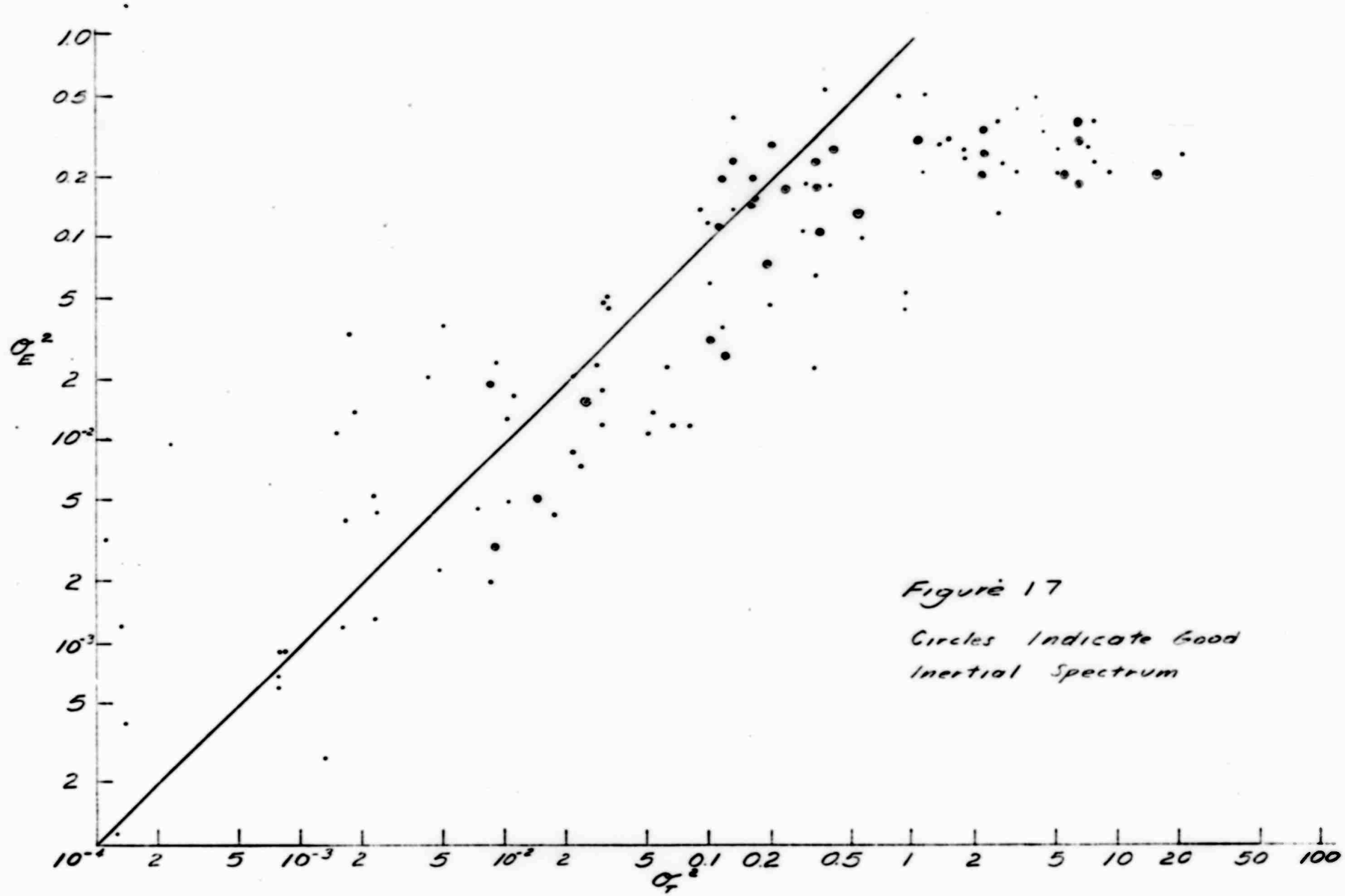

Figure 17

Circles Indicate Good Inertial Spectrum

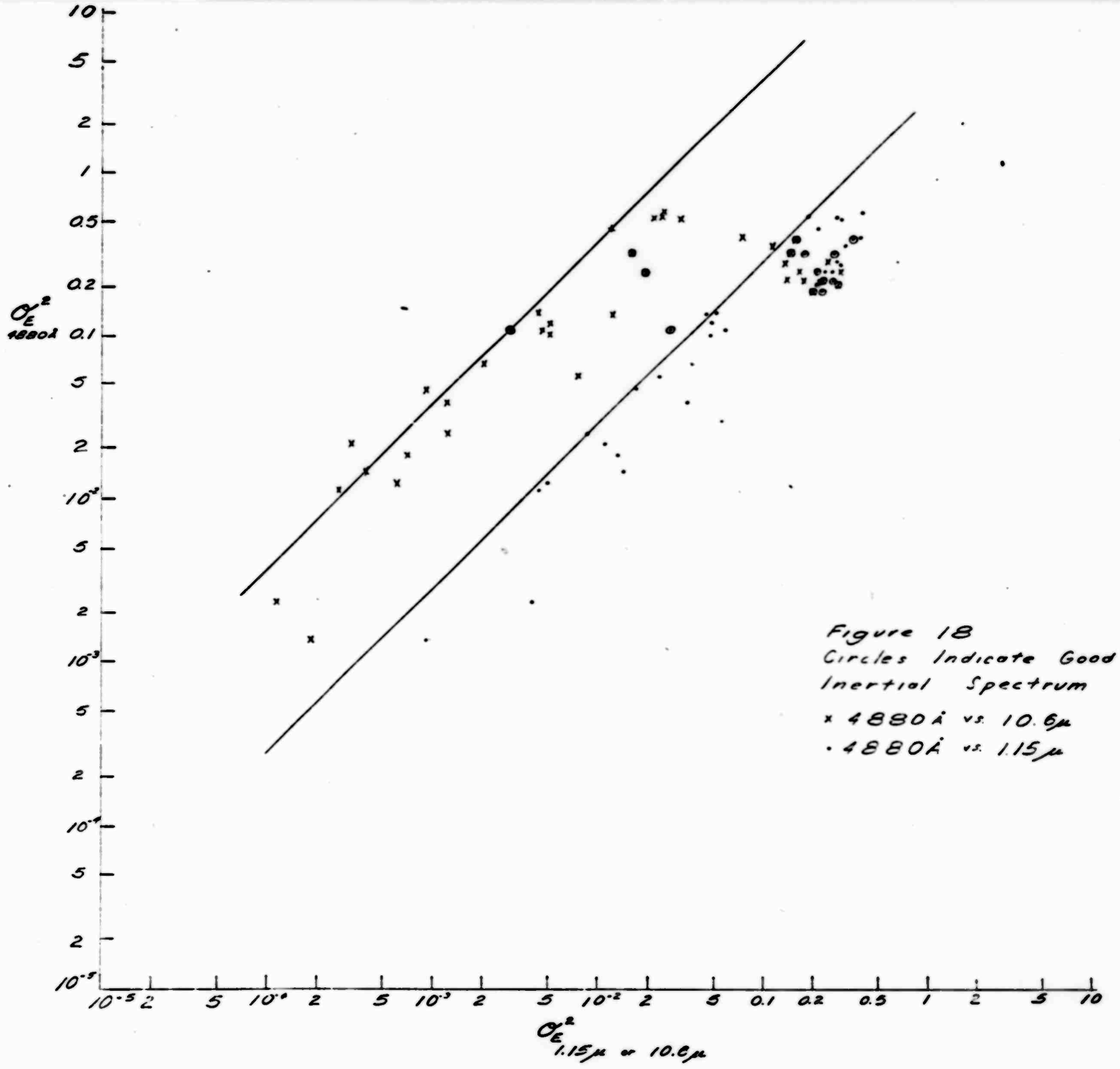

Figure 18
Circles Indicate Good
Inertial Spectrum
× 4880Å vs. 10.6μ
· 4880Å vs. 1.15μ

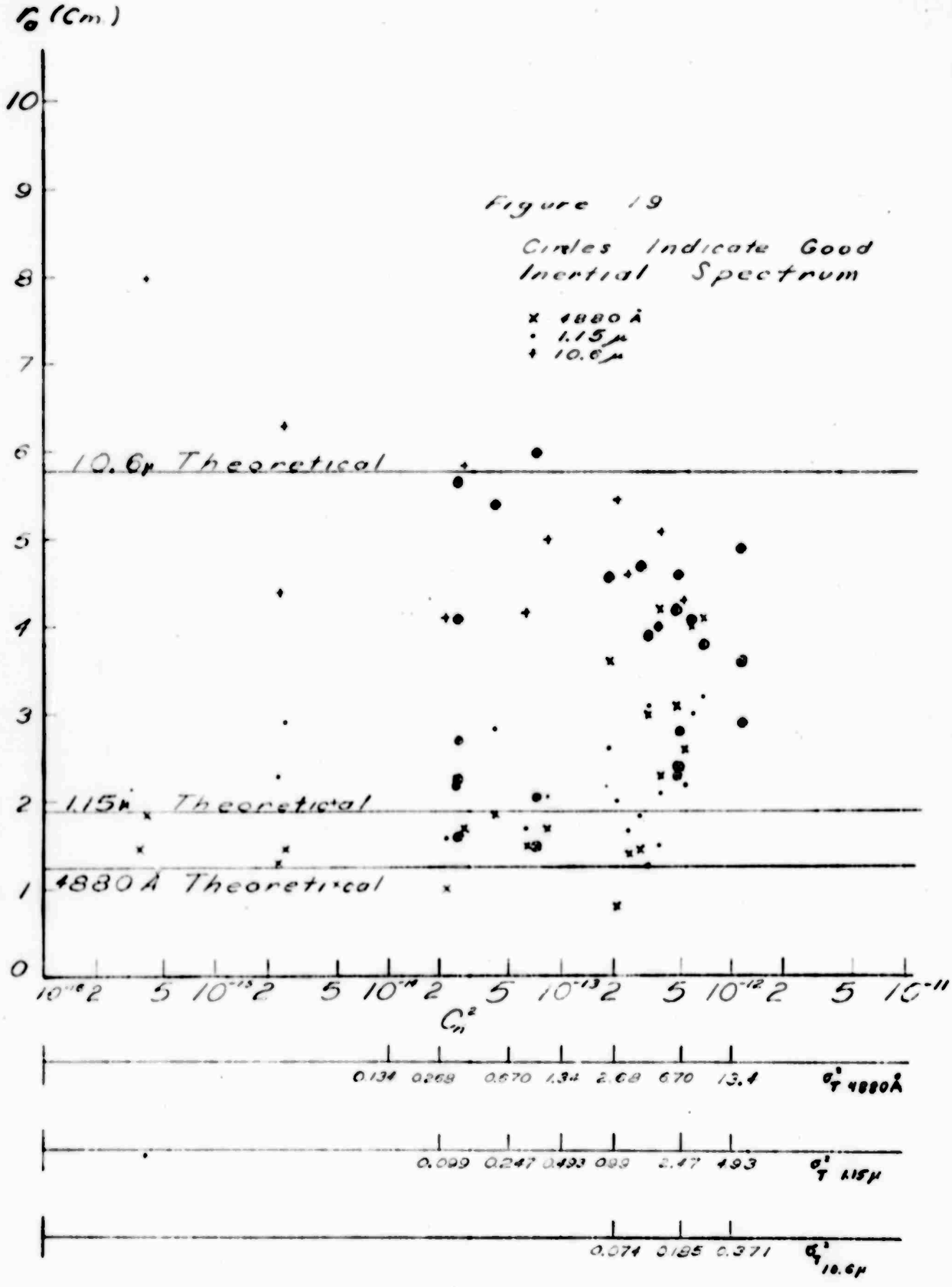

Figure 19

Circles Indicate Good Inertial Spectrum

× 4880 Å
· 1.15μ
+ 10.6μ

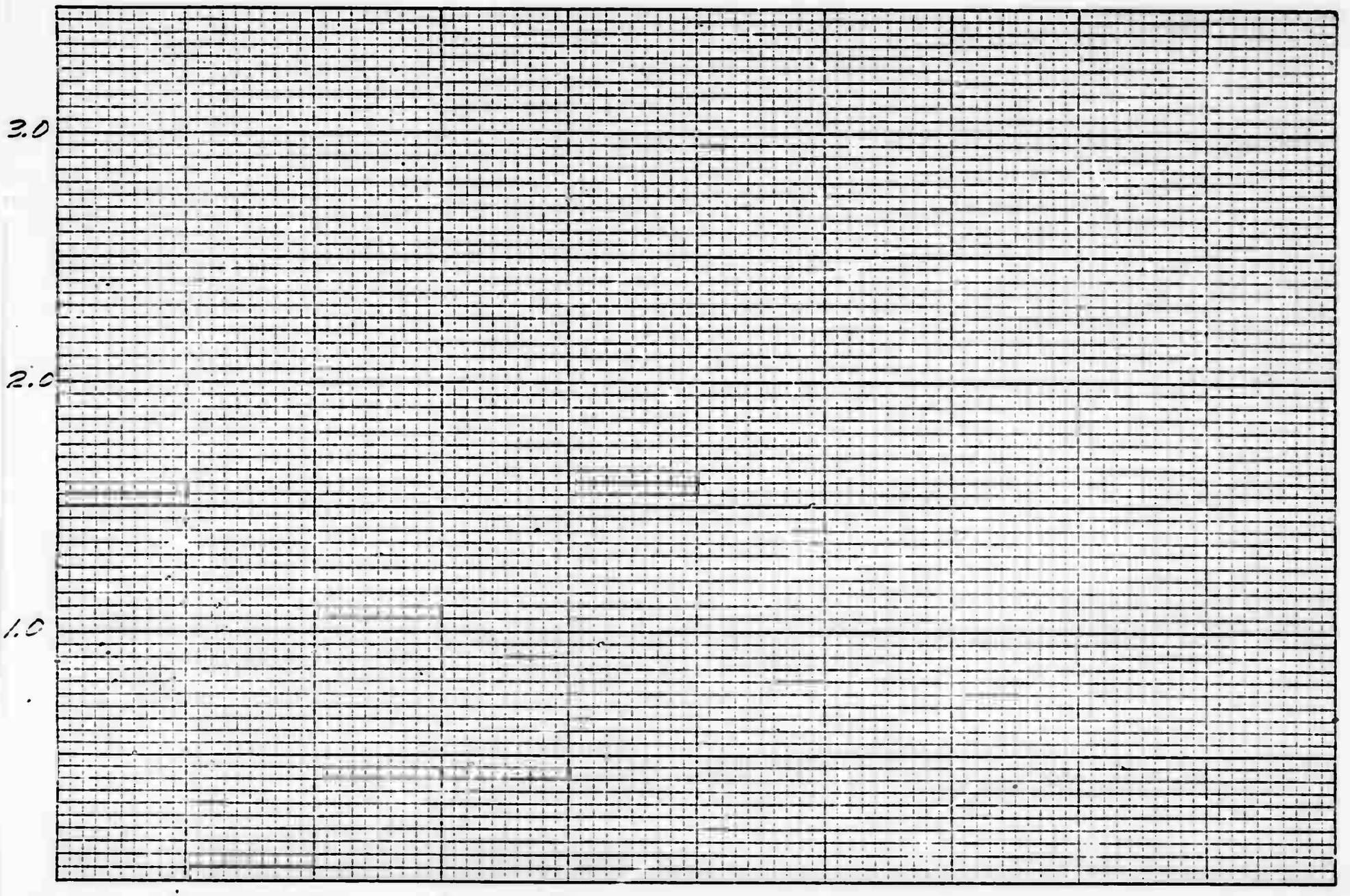

Figure 20.

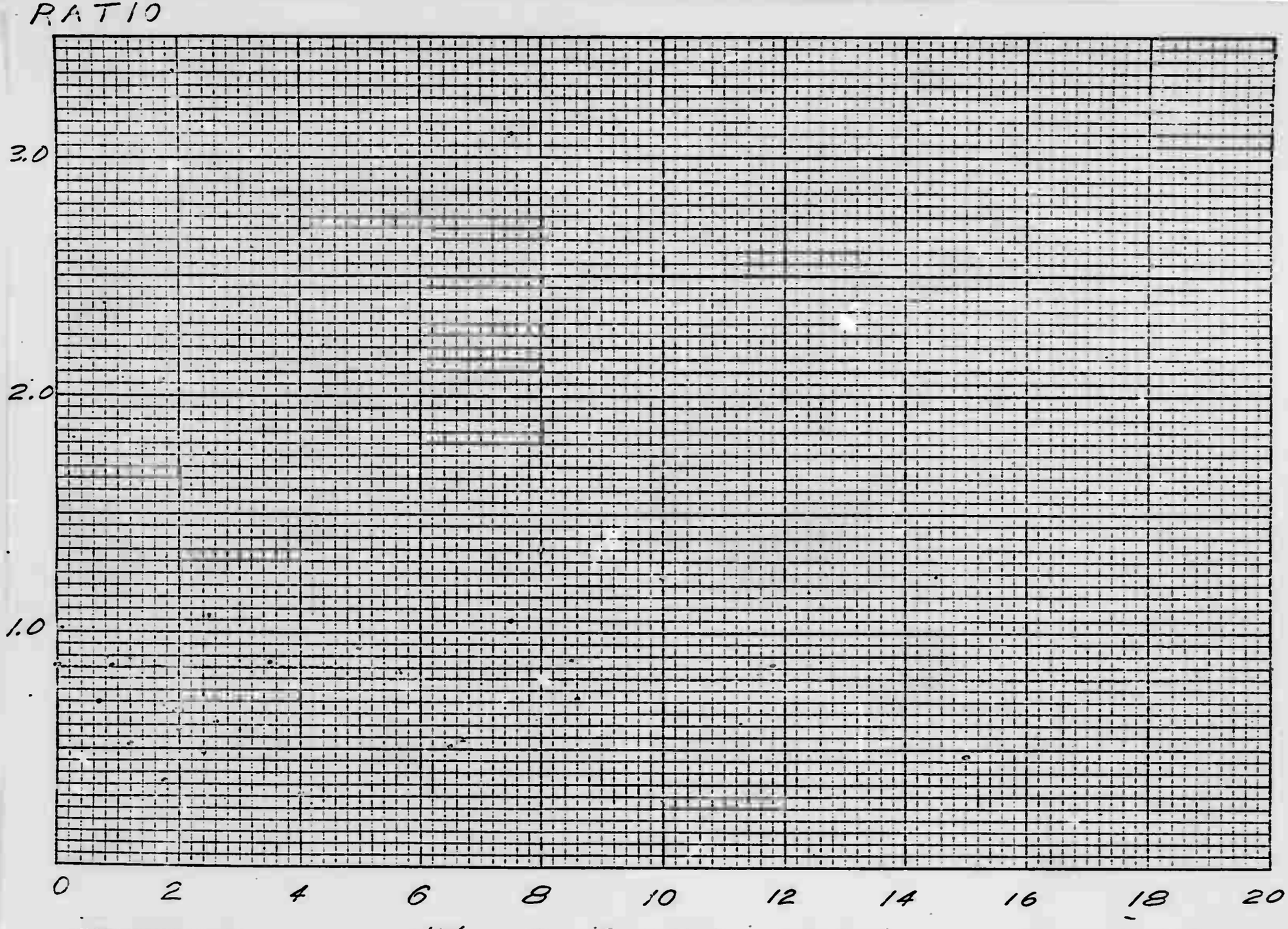

Figure 20b

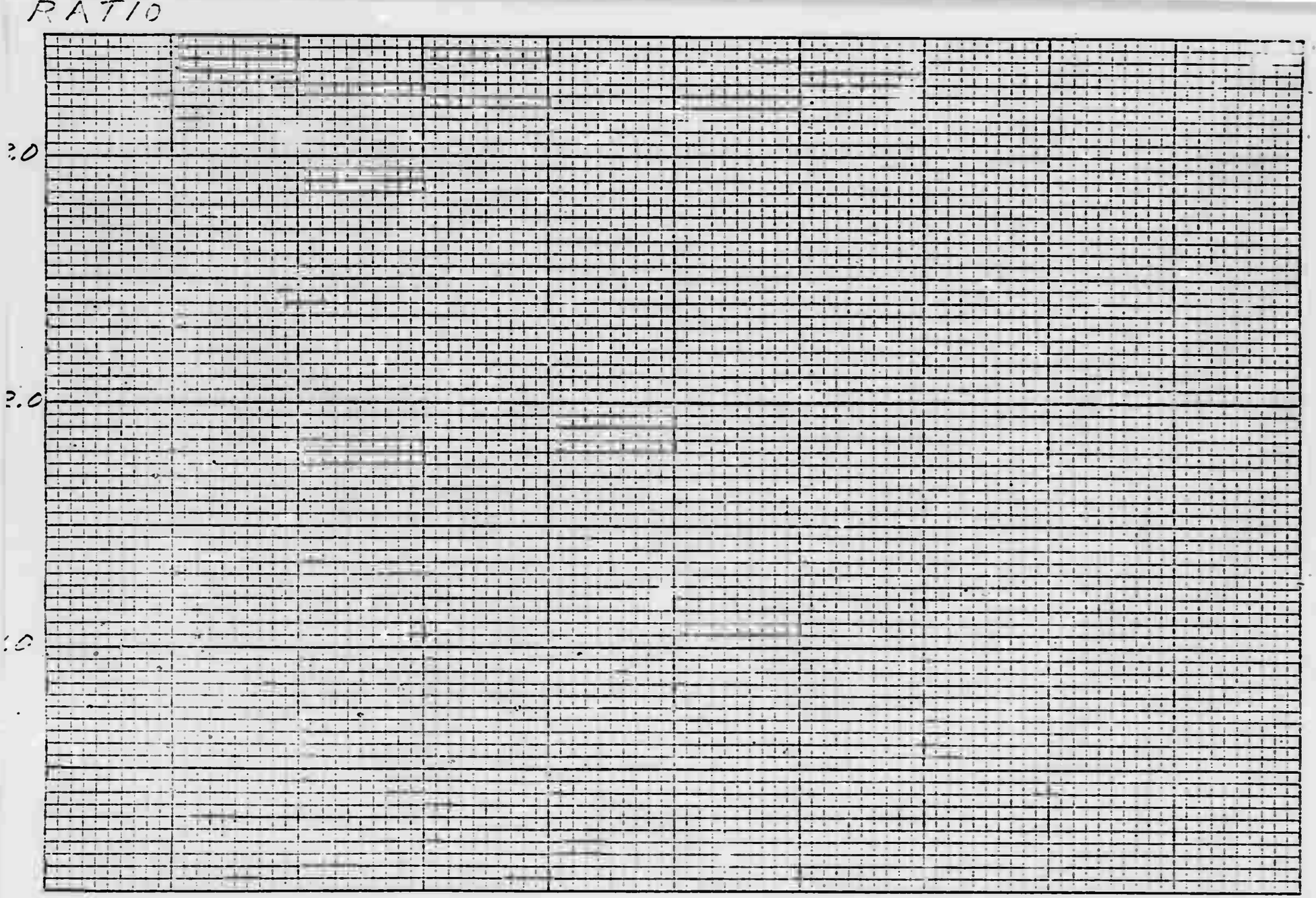

Figure 20c

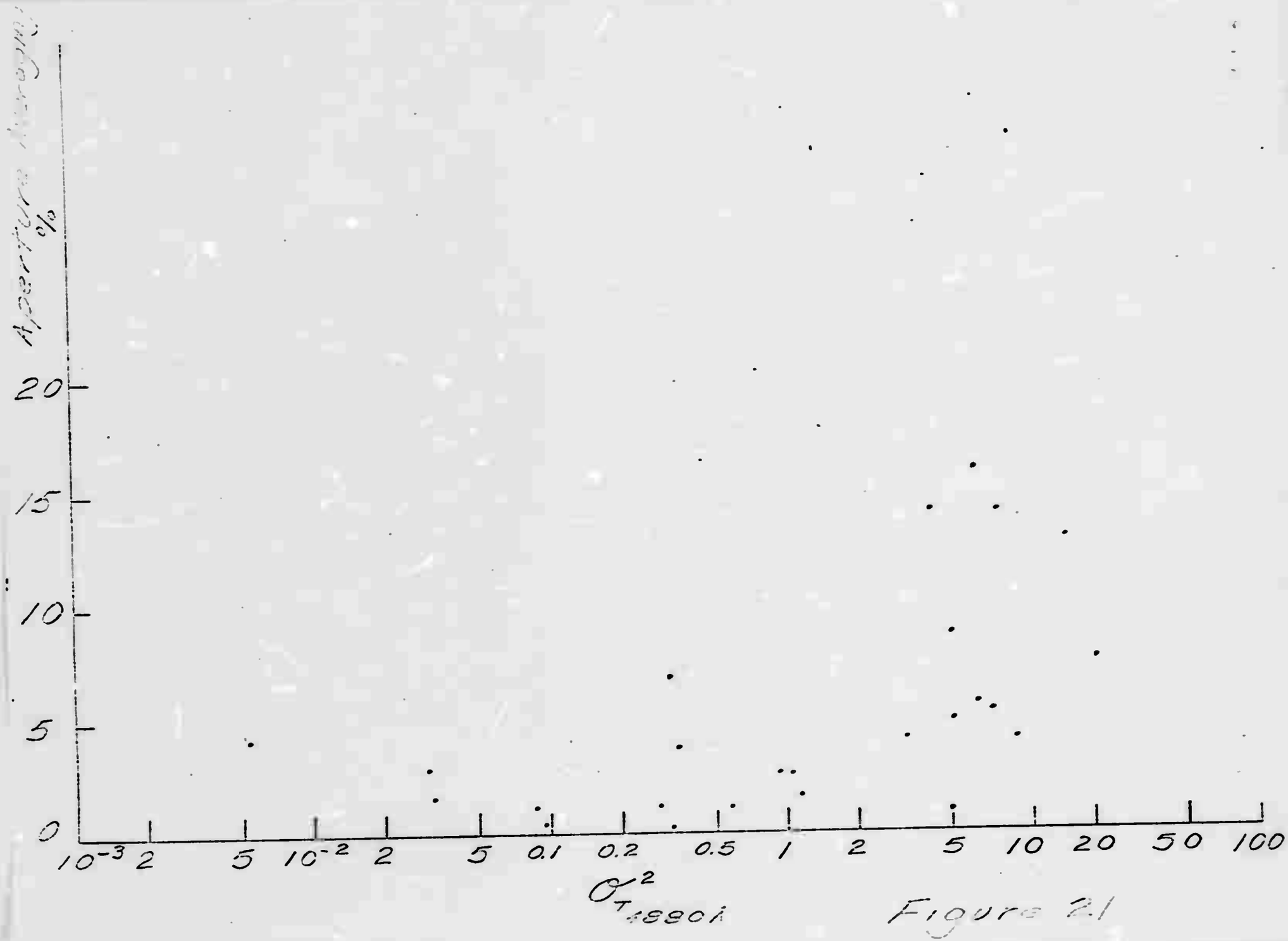
Modulation Amplitude %
20
15
10
5
0
10^{-3} 2 5 10^{-2} 2 5 0.1 0.2 0.5 1 2 5 10 20 50 100
$\sigma^2_{T\,4890\text{Å}}$

Figure 2.1

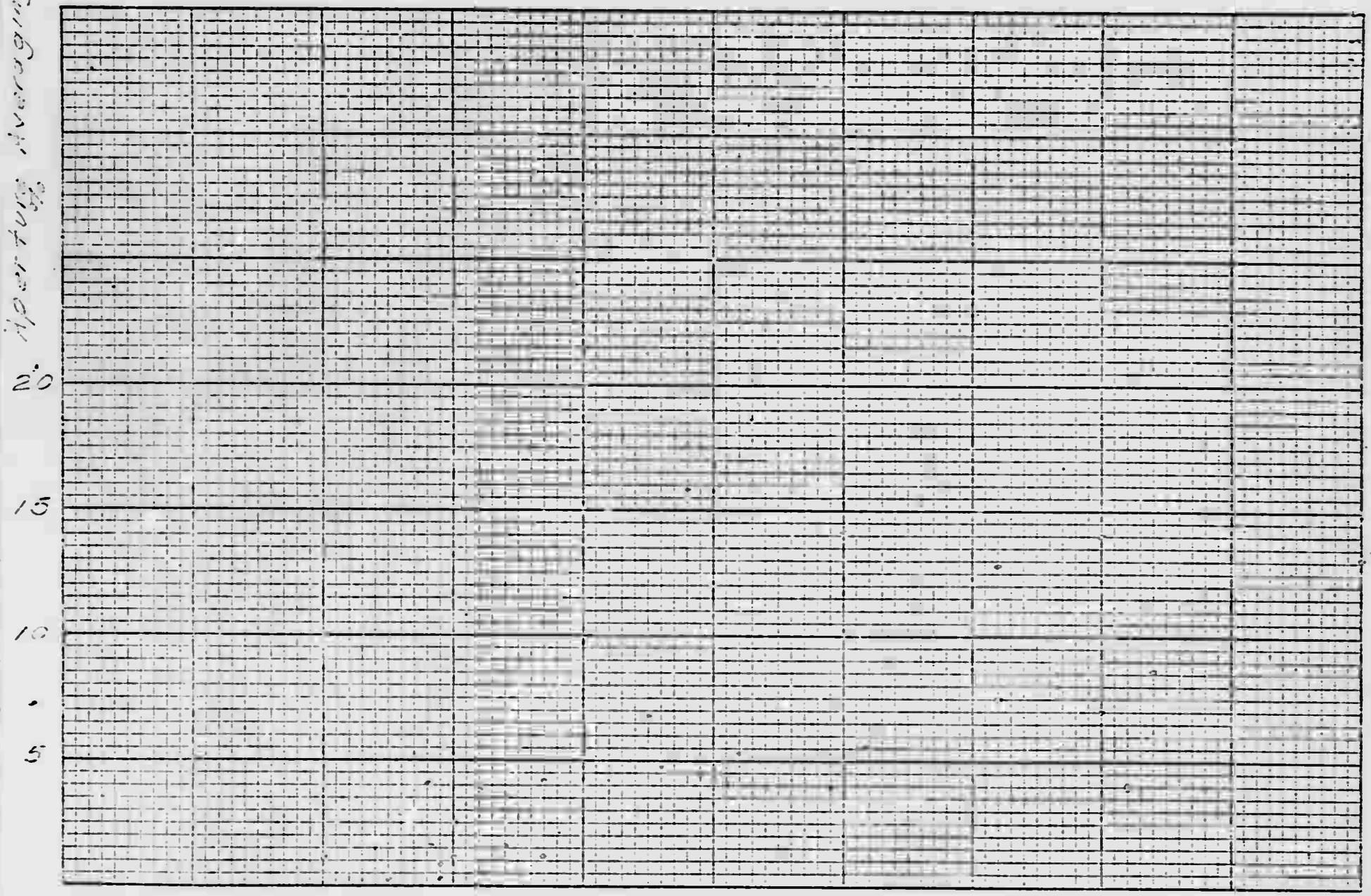

Figure 22

(Unclassified)

Security Classification

DOCUMENT CONTROL DATA - R & D

Security classification of title, body of abstract and indexing annotation must be entered when the overall report is classified

1. ORIGINATING ACTIVITY (Corporate author) Oregon Graduate Center 9340 SW Barnes Rd. Portland, Oregon 97225	2a. REPORT SECURITY CLASSIFICATION Unclassified 2b. GROUP

3. REPORT TITLE

MULTIWAVELENGTH LASER PROPAGATION STUDY---III

4. DESCRIPTIVE NOTES (Type of report and inclusive dates)
Quarterly: September 16, 1970--December 15, 1970

5. AUTHOR(S) (First name, middle initial, last name)

J. Richard Kerr

6. REPORT DATE	7a. TOTAL NO. OF PAGES	7b. NO. OF REFS
January, 1971	48	13

8a. CONTRACT OR GRANT NO.	9a. ORIGINATOR'S REPORT NUMBER(S)
N00014-68-A-0461-0001 b. PROJECT NO.	1154-10
c.	9b. OTHER REPORT NO(S) (Any other numbers that may be assigned this report)
d.	

10. DISTRIBUTION STATEMENT

Distribution of this document is unlimited.

11. SUPPLEMENTARY NOTES	12. SPONSORING MILITARY ACTIVITY
	Advanced Research Projects Agency Department of Defense--Pentagon Washington, D.C. 20301

13. ABSTRACT

An extensive experimental investigation of multiwavelength laser beam scintillations and atmospheric turbulence characteristics has been completed. It has been found that turbulence spectra approximate the inertial-subrange model only under conditions of strong turbulence, which corresponds with saturation of scintillations at visible and near-IR wavelengths. Hence, it is only at longer wavelengths (such as 10.6 microns) that Rytov analyses utilizing the inertial subrange have substantial value.

The saturation phenomenon occurs at the same scintillation levels independent of wavelength, and significant falloff of scintillation "beyond saturation" is observed. Covariance measurements show transverse amplitude correlation lengths which are significantly affected by strong turbulence; the correlation lengths increase at shorter wavelengths while decreasing at longer wavelengths, as turbulence increases. Receiver aperture-averaging results at visible wavelengths show that the large-aperture smoothing of total-signal fluctuations is much less effective than theoretically predicted, and confirm the especially-poor averaging in strong turbulence conditions.

14. KEY WORDS	LINK A		LINK B		LINK C	
	ROLE	WT	ROLE	WT	ROLE	WT
Visible atmospheric transmission Infrared atmospheric transmission Turbulence scattering Atmospheric propagation						